Summer 2022

A Study of Cobalt (III) Oxide Nanoparticle Delivery of siRNA Molecules Directed Against Signaling Intermediates of the P2Y2 Receptor

Rachel Blair Stroud
Missouri State University, RachelStroud@MissouriState.edu

A STUDY OF COBALT (III) OXIDE NANOPARTICLE DELIVERY OF siRNA MOLECULES DIRECTED AGAINST SIGNALING INTERMEDIATES OF THE $P2Y_2$ RECEPTOR

A Master's Thesis

Presented to

The Graduate College of

Missouri State University

In Partial Fulfillment

Of the Requirements for the Degree

Master of Science, Cell and Molecular Biology

By

Rachel Blair Stroud

August 2022

A STUDY OF COBALT (III) OXIDE NANOPARTICLE DELIVERY OF siRNA MOLECULES DIRECTED AGAINST SIGNALING INTERMEDIATES OF THE $P2Y_2$ RECEPTOR

Biomedical Sciences

Missouri State University, August 2022

Master of Science

Rachel Blair Stroud

ABSTRACT

G protein-coupled receptors are evolutionarily ubiquitous sensors of extracellular signals, propagating intracellular signal cascades through heterotrimeric G proteins. $P2Y_2$ receptors are GPCRs which are activated by extracellular nucleotides to mediate signaling cascades via $G_{\alpha q}$ coupling. Many GPCRs are subject to a common mechanism for signal termination involving phosphorylation of the C-terminal tail followed by β-arrestin binding and subsequent endocytic internalization of the complex. This effect has been described for the $P2Y_2$ R in the 1321N1 astrocytoma cell line, and UTP-induced activation and desensitization profiles have been previously defined. There is need to develop molecular vehicles for safe and effective delivery of nucleic acids such as siRNA, a therapeutic target largely unrealized. Cobalt (III) Oxide nanoparticles, chosen due to preliminary success, were used to deliver β-arrestin1 siRNA to 1321N1 cells. MTT assay shows Co_3O_4NP are not toxic in this cell line. No baseline for β-arrestin1 expression could be established during qRT-PCR, as such neither Lipofectamine™ nor Co_3O_4NP delivery of the siRNA conferred measurable knockdown. Calcium assays reveal no significant differences between desensitization proficiency with or without siRNA, though there is visible grouping between treatments. Similarly, unexpected wild type dose-response desensitization trends complicated calcium assay analysis, such that previously reported behavior could not be replicated. Overall, no significant trends were observed, and further trials will be required, largely due to the difficult nature of working with these inorganic nanoparticles.

KEYWORDS: $P2Y_2$ receptor, nucleotide signaling, β-arrestin, cobalt (III) oxide nanoparticles (Co_3O_4NP), siRNA, nucleic acid delivery, qRT-PCR, calcium assay, G protein-coupled receptors (GPCR)

A STUDY OF COBALT (III) OXIDE NANOPARTICLE DELIVERY

OF siRNA MOLECULES DIRECTED AGAINST

SIGNALING INTERMEDIATES

OF THE $P2Y_2$ RECEPTOR

By

Rachel Blair Stroud

A Master's Thesis
Submitted to the Graduate College
Of Missouri State University
In Partial Fulfillment of the Requirements
For the Degree of Master of Science, Cell and Molecular Biology

August 2022

Approved:

Richard Garrad, Ph.D., Thesis Committee Chair

Randi Ulbricht, Ph.D., Committee Member

Jianjie Wang, Ph.D., Committee Member

Julie Masterson, Ph.D., Dean of the Graduate College

ACKNOWLEDGEMENTS

I've thought about this dedication a lot, and no matter what I say, words seem to fall short of expressing the gratitude I owe to so many - teachers, family, friends. Despite some interesting struggles, I'm finally here, and none of this would have been possible without support from so many incredible people in my life.

To my committee, Dr. Garrad, Dr. Ulbricht, and Dr. Wang, thank you so much for your continued support, expertise, guidance, and unending patience through this entire process.

To my parents, and to my family, thank you for always supporting and encouraging me throughout my education!

Ben, thank you for being exactly what I need; kindness, stability, distraction, and underrated reminders to 'get back to work'.

Finally, to the Biomedical Sciences Department, faculty, staff, students past and present, thank you! My time here has been such an incredible opportunity for me to grow as a scientist, professional, and individual and it has much to do with the passion and dedication I've found in The Biomedical Sciences Department.

TABLE OF CONTENTS

LIST OF TABLES

LIST OF FIGURES

INTRODUCTION

G Protein-coupled Receptor Superfamily

G protein-coupled receptors (GPCR), the largest gene family of membrane-bound receptors, are an ancient signaling solution to the dilemma of environmental awareness under the protective limitations of membrane permeability. These receptors contain 7 α-helical stretches that weave through the membrane, leaving 3 loops on either side. On the extracellular surface these loops form binding pockets responsible for ligand recognition, after which a conformational shift across the membrane in the 3rd and 6th helices allows for coupling of the intracellular loops and C-terminal tail to a membrane-bound heterotrimeric G-protein (1–5).

Variability in distribution, signal transduction and gross physiologic effects are represented by each GPCR family member. GPCRs boast seven membrane-spanning helical domains, therefore are also referred to as seven transmembrane receptors. To date, the primary classification method splits the superfamily of human proteins into five groups, based on sequence homology and functional (signaling) outcomes. Class A/rhodopsin-like GPCRs are the largest and most studied class, with characterization efforts in the 1980's including rhodopsin and β2-adrenergic receptors (6). Other noteworthy Class A families include chemokine receptors, important for signal transmission in the immune system (7) opioid receptors, involved in antinociception (8), and P2Y receptors, a family with 8 members capable of recognizing adenosine and uridine nucleotides (9). Class B receptors, historically have been split into 2 subgroups; B1 for hormones including secretin and glucagon and B2 for adhesion receptors, several of which interact with integrins (10). Class C includes neuromodulating metabotropic glutamate and GABA receptors (11, 12). Class F is composed of the Frizzled receptors, extensively studied in *Drosophila melanogaster*, shown to be involved in early development as

well as some cancer progression (13). Two final groups, Class D, fungal mating pheromone receptors, and class E, cyclic adenosine monophosphate (cAMP) receptors have not been identified in vertebrates. With such a large family, new members are being defined and characterized regularly. Still, there are a number of 'orphan receptors' whose endogenous ligands have yet to be identified, and those that seem to defy current groupings all-together (14, 15).

GPCR Signal Transduction

Primarily stimulatory effects are noted from receptors linking to $G_{\alpha s}$ which activates adenylyl cyclase, responsible for increasing intracellular cAMP concentration ([cAMP]), and downstream activation of Protein Kinase A (PKA), a cAMP-dependent protein kinase. $G_{\alpha i/o}$ -linked receptors exert inhibitory effects on adenylyl cyclase producing downstream dampening of cAMP-dependent pathways. Related are the $G_{\alpha t}$ group, specifically involved in sensory transduction. $G_{\alpha q/11}$ activation is responsible for activation of phospholipase C-β (PLC-β) leading to cleavage of membrane lipid phosphatidylinositol 4,5-bisphosphate (PIP_2) into inositol 1,4,5-trisphosphate (IP_3) and diacylglycerol (DAG) constituents, mobilizing endoplasmic reticular Ca^{2+} stores and activating Protein Kinase C (PKC), respectively (16). The Rho-guanine nucleotide exchange factor (Rho-GEF) family is activated by $G_{\alpha 12/13}$ proteins, a signaling cascade responsible for dynamic cytoskeleton rearrangement implicating them in regulation of cellular growth, motility and apoptosis (17).

Truly, classical descriptions of receptor signaling outcomes are derived from α-subunit-related signaling events. However, it is important to note that, in addition to post-translational lipid modifications for membrane targeting of the heterotrimeric G protein complex (18), the corresponding βγ dimers are also able to elicit activation of a number of downstream signaling

cascades. In humans, 5 β isoforms and 11 γ isoforms have been identified, most of which are capable of dimerization, with signaling outcomes and efficacy highly specific to the pair. Some downstream effector cascades include ion channels (19), PLC-β(20) and mitogen activated protein kinases (MAPKs) (21, 22).

The effector molecules to which G_α proteins couple promote a number of signaling cascades of their own and are thus understood to be secondary signaling molecules (second messengers) within the pathway of receptor signal transduction. For example, Ca^{2+} release from the endoplasmic reticulum is one such activated effect of the β2-Adrenergic Receptor (β2AR) and many other GPCRs. Additionally, subsequent steps within a signal cascade are often subject to some level of amplification, therefore, second messengers such as these make for ideal quantitation of the effects of receptor stimulation. While absolute ligand-binding and receptor-activation (*G protein activation*) are much more challenging to measure directly, clever genetic modifications have allowed for the use of fluorescence/bioluminescence-resonance energy transfer (FRET/BRET) -based studies, revealing spatial and temporal features of GPCR signal cascades (23, 24).

Purinergic Receptors

With so many unique receptors, the number of molecules recognized that can elicit a response is functionally infinite. The nucleotide adenosine triphosphate (ATP) is a ubiquitous molecule; intracellular proteins capable of ATP synthesis and hydrolysis are both fundamental to all known life. Not only is it the major source of energy and a precursor for synthesis of nucleic acids and cAMP, ATP is an extracellular signaling molecule. It should come as no surprise that these intra- and extracellular mechanisms of interaction with ATP occurred early in evolutionary

history, evidenced by the quantity and diversity of organisms which possess the molecular machinery (25–27).

At the base of the ATP structure is the nucleoside adenosine, classified as a purine due to its heterocyclic structure. Around the 1930's, characterization efforts began in earnest to delineate the ability of adenosine and other extracellular nucleotides to modulate intracellular signaling. These events were first described as 'purinergic signaling' by Burnstock in the early 1970s, although it was later determined that pyrimidines such as uridine triphosphate (UTP) also elicit physiologic changes (28, 29). Still, the term persists, and purinergic signaling is now known to occur in most cells. The earliest studies of this 'non-adrenergic, non-cholinergic nerve transmission' necessarily focused on nervous tissues and as such purinergic signaling has been described extensively in cells of the central and peripheral nervous systems. Purine and pyrimidine nucleotides may be released from apoptotic cells through caspase signaling to serve as a 'damage signal' (30). The extracellular nucleotides act on nearby cells to initiate a protective response, also inducing chemotaxis in monocytes and macrophages to the area to prevent further spread of the damaging stimulus (31–33).

In a recent 2018 review, Burnstock identifies three major receptor families with respect to purinergic signaling: P1, P2X and P2Y receptors (9). There are four P1 receptor subtypes, all of which bind extracellular adenosine nucleotides to exert modulatory effects on the production of intracellular cAMP via coupling to $G_{\alpha s}$ or $G_{\alpha i/o}$ effectors in a subtype specific manner (34).

Members of the P2 family of receptors recognize extracellular nucleotides such as ATP and UTP, in addition to the di- and monophosphate versions of these molecules. P2X receptors are ligand-gated ion channels (LGIC) which, upon binding these nucleotides, open to allow passage of cations across the cell membrane. There are seven family members, consecutively

named $P2X_{(1\text{-}7)}$ of which $P2X_{1,2,4}$ preferentially allow Ca^{2+} efflux (35). P2X receptors also have a propensity toward heterodimerization. The exact receptor subtypes which couple together expand the signaling repertoire of the family immensely.

P2Y receptors are GPCRs named non-consecutively, all members play some role in phospholipase activation through coupling to G-$\alpha_{q/11,}$ except for $P2Y_{12}$, which couples to G-α_i, inhibiting downstream production of cAMP. Notably, one family member, the $P2Y_2R$, responds with equal efficacy and potency to ATP and UTP, both lead to activation of the coupled G-α_q followed by activation of the PLC-β signaling cascade described previously. In addition to canonical G protein signaling, most P2Y family members have been shown to couple to extracellular signal-regulated kinase 1/2 (ERK 1/2), a MAPK, however the exact outcome is highly cell-type and environment specific. This is probably due to concerted and differential efforts from multiple contributing P2Y receptor types for any given extracellular nucleotide signaling event (36–39).

While signaling of these receptors is important, regulation has equally profound physiological implications. In the central and peripheral nervous system, nucleotide release and the subsequent intracellular signaling cascades modulated by purinergic receptors are often the result of physical or chemical damage (30, 40). These signals are largely proinflammatory, promoting reactive astrogliosis and interplay with downstream effectors like arachidonic acid (prostaglandin E2), NF-κB, and cytokines (interleukins, TNF-α) which should help to isolate and resolve the damage (37, 41). Prolonged stimulation of purinergic pathways can lead to chronic inflammation which can display deleterious effects on the system (42). Extracellular nucleotides act on nearby cells since extracellular nucleotidases often degrade local signals before reaching more distant cells. Another way these signals are closely regulated is by sequestration of

membrane-bound purinergic receptors through physical removal from the plasma membrane in an β-arrestin-dependent fashion. Prototypical GPCR signal termination has been studied with the $P2Y_2R$ in cultured 1321N1 human astrocytoma cell line, stably transfected with HA-tagged, murine $P2Y_2R$ (43, 44).

GPCR Signal Termination

In a 2006 *Molecular Cell* review, Lefkowitz *et al.* identified 3 critical interactions, collectively and constitutively regulating every explored instance of agonist-induced GPCR signaling (45). Outlined in Fig. 1, Upon stimulation by extracellular ligand, the cytosolic third intracellular loop and C-terminal tail of the receptor are susceptible to phosphorylation by a G protein-coupled receptor kinase (GRK) (46). The phosphorylated tail of the receptor interacts with a β-arrestin scaffolding protein, directing the complex into Clathrin-coated pits (CCP) for the purpose of endocytosis (47). Clathrin adapter protein AP2 has a β-arrestin binding domain, functionally linking the receptor to the clathrin-lattice and ensuring it is internalized through formation of the early endosome (Fig. 2A). As the CCP matures, the associated membrane segment becomes further invaginated until dynamin, a motor protein, can encircle the remaining opening and seal off the end. Once internalized, the receptor and interacting components may be re-primed and recycled to the plasma membrane for further signaling, they may be degraded, or they may still be responsible for further signaling events (Fig. 1).

As the first step in regulation of GPCR signaling, GRKs play a substantial role within tissues, conveying major physiologic impacts. There are seven human GRKs, each with conserved structure and the potential for post-translational modifications unique to certain subtypes (Fig. 2B). The basic structure of all GRKs is comparable, with an N-terminal RGS-like

domain, central catalytic domain, and a C-terminus that varies between family members. GRKs 1. and 4-7 possess C-terminal lipid modifications (*palmitoylation & farnesylation*) which are vital for membrane localization (48–50). GRKs 2 and 3, also known as β-adrenergic receptor kinases (βARKs) were first discovered interacting with the β-adrenergic receptors, as the original naming would suggest. Following identification of these two, other family members as well as other receptor binding partners were discovered. These two family members are unique, with C-terminal β/γ-binding capabilities shown to contribute to membrane localization (51). GRKs are vital for homeostatic control of G protein-coupled receptor signaling throughout the body. For example, human blood pressure homeostasis is highly dependent on GRK regulation of multiple receptors involved in vascular tone and blood volume (52). Specifically implicated in the control of vascular tone and/or blood pressure are the angiotensin-II receptor, type 1 (AT_1R), α- and β-adrenergic (α-, β-AR), endothelin A and B receptors ($ET_{A/B}R$), Neuropeptide Y, acetylcholine receptor (AChR) and dopamine receptors. Signaling of each of these receptors is closely regulated by GRKs (53).

β-arrestins: Receptor Internalization & Other Signaling Implications

Arrestins are a protein family found in archaea and eukaryotes composed of α-arrestins, β-arrestins and Vps26 (54). Receptor sequestration and the potential for resensitization and recycling is dependent upon the type of interaction between the GPCR and the β-arrestin. In 2000, Oakley *et al.* defined two classes of regularly observed receptor-arrestin interactions. The first group, which includes the β2-adrenergic receptor (β2AR), has greater affinity for β-arrestin2 (arrestin-3) than for β-arrestin1 (arrestin-2) (55). However, the half-life of this receptor-arrestin complex is short-lived, and the receptors in this class are re-primed and returned to the

membrane relatively quickly. The second class, which includes the vasopressin 2 receptor (V2R), displays a sustained interaction with comparable affinity for both β-arrestins, and is marked by prolonged periods of internalization and a greater potential for degradation under these conditions. Studies in 2016 from Thomsen et al. and 2017 from Cahill et al. produced a chimeric V2R in which the native C-terminal domain was replaced with the C-terminus of the β2AR (β2V2R). These studies showed a complete switch of receptor behavior under prolonged agonist stimulation, where the β2V2R -arrestin interaction was transient, and these chimeric receptors were more quickly returned to the membrane, as is common with the native β2AR (56, 57).

Seemingly disparate signaling outcomes can initiate from the same GPCR-binding, extracellular signaling molecule. Much effort has gone into describing the role of β-arrestins in these signaling outcomes, and the discovery that GPCR ligands can have variable efficacies with regards to both G protein and β-arrestin signaling was a confounding and vital step toward the latest advances. The term 'biased ligand' is used to describe unique GPCR-ligand pairs with intrinsic propensity toward specific 'active conformations' and the corresponding signaling outcomes. Examples of 'perfect-bias', when ligand-binding activates only one of these effector pathways (G protein, or β-arrestin) have been used to delineate the importance of this relationship. This situation is not expected to occur with many endogenous ligands; a more likely story is the use of multiple 'imperfectly-biased' molecules to weakly target desired subsets of signaling outcomes (58, 59).

Studies with the μ-opioid receptor (μOR) provided further evidence that the specific β-arrestin interaction is important for downstream signaling events. Importantly, these studies were the first to highlight the phenomenon of 'arrestin biased-ligands'. While the endogenous μOR

enkephalin ligands stimulate G protein and β-arrestin signaling equipotently, morphine, a negative-arrestin-biased ligand, is found to strongly induce G protein signaling, and to a much lesser degree β-arrestin signaling. Early studies with β-arrestin mutant mice were used to show the significance of arrestin-bias at μOR, particularly its roles in some undesirable, even dangerous side-effects and tolerance associated with μOR ligands (60, 61). This information may be important as most clinical pain is treated with synthetically derived opioid receptor ligands. Additionally, many other modern pharmaceuticals and receptors have already been shown to exhibit biased-signaling mechanisms by which G protein and β-arrestin signaling are potentiated to varying degrees (58)**.**

Nanotechnology in Biological Applications

Over the past several decades, nanotechnology has entered a new era of expansive growth. Nanoparticles are defined as having a size less than 100 nm. Nanoparticles have applications in many fields including physics, manufacturing, physical chemistry, and biology. In biology there are many types of materials used for nanoparticles; some of the most common include lipids, proteins, organic and inorganic molecules (62). Additionally, any of these materials can be individually modified, or conjugated with the others, changing the biological activity and significantly increasing the functional repertoire of these biologically useful nanoparticles.

To date, many inorganic metals have been used as nanoparticles. Inert gold and silver are common, but metal oxides have also earned a place in the field of nanobiotechnology. Some of the most intriguing nanoparticle choices for biological research are the heavy metals, many of which naturally serve as enzymatic cofactors, but will become toxic in conditions of high

exposure. One such metal that has garnered interest in the field of nanobiotechnology is cobalt. As a transition metal, it has two oxidation states, which gives rise to three potential nanoparticles formulations: Cobalt nanoparticles (CoNP), Cobalt (II) Oxide nanoparticles (Co_2O_3NP), and Cobalt (III) Oxide nanoparticles (Co_3O_4NP). Each formulation exhibits different behaviors in biological situations, one notable feature is that CoNP and Co_2O_3NP which have a functional Co^{2+} surface chemistry, are relatively soluble and highly toxic in cell culture as indicated by decreased cell viability, increased reactive oxygen species production, and DNA damage. In contrast, the same study noted little-to-no toxicity from Co_3O_4NP using the same indications. This is due in part to the leaching of cobalt ions (Co^{2+}) by CoNP and Co_2O_3NP into cell medium containing serum (63). A 2014 screen identified Co_3O_4NP have the potential for efficient delivery of RNA inside of the cell, though the precise mechanism by which they readily cross the membrane has yet to be defined (64, 65).

Nanoparticle size and surface architecture are vital for it to be an effective carrier for any nucleic acid therapeutic. Many methods of characterization have been developed; however, electron microscopy (SEM or TEM) remains one of the most used methods for verification of nanoparticle size. Another important factor to consider for nanoparticle use for intracellular delivery of organic materials is the conjugation to the material. For this, Hurst and Delong worked to produce a technique called 2D-fluorescence difference spectroscopy. This technique uses the basic principles of spectroscopy to create a unique ‘spectral signature’ excitation/emission profile for bare nanoparticles. Once conjugated to biomaterials, these nanoparticles adopted a measurable ‘shift’ in the signature, allowing for confirmation of the interaction (66).

An organism must be able to sense and respond to changes in its environment. While this is certainly true at the organismal level, it is also essential at the cellular level. The presence of a membrane encasing each cell complicates the ability of the cell to interact with the extracellular environment. The membrane is fastidious in its scrutiny over membrane transport, and with good reason: many cells contain molecular machinery common to most life, which can even be used against the native cell in the event of internalizing xenobiotics, including but not limited to intracellular parasites and viruses. As a testament to this barrier, most modern pharmaceuticals still work from the outside of a cell, and by targeting transmembrane receptors, most commonly GPCRs.

Small interfering RNA (siRNA) has become an indispensable tool for many studies in cell biology. The technique involves exogenously sourced double-stranded RNA (dsRNA) complementary to a transcript of interest. RNA-induced silencing complex (RISC) within the cytoplasm of the cell initiates an interaction with the matching cellular mRNA based on short 21-23 nucleotide segments, triggering degradation and/or preventing translation of the target (67). A primary limitation to this method is delivery of RNA across the membrane and to the cytoplasm of the cell. RNA is relatively unstable and crossing the cell membrane is a process which not every molecule can accomplish. Methods to protect RNA while also allowing it to selectively pass into targeted cells readily must be developed before the full potential of this technique may be realized, both in the lab and clinic.

Previously, siRNA targeted knockdown of β-arrestin1 and GRK2 have both shown significant knockdown in the 1321N1 astrocytoma cell line, with no inhibitory effects on downstream regulation of GPCR signal as observed by calcium assay (68). These trials highlighted Lipofectamine^{TM}, an industry standard transfection reagent, as an effective vehicle

for delivery of siRNA into the cell line and will provide a tool for comparison of other potential vehicles for delivery of siRNA.

Goals and Aims

The action of β-arrestin proteins is directly related to termination of GPCR signaling through the process of desensitization and sequestration. This has been shown widely and consistently through modulation of its expression (69). With such power over such a large family of proteins expressed throughout all tissues of the body, there is obvious therapeutic merit in designing a targeted delivery system for nucleic acids capable of modulating β-arrestin expression. Previously, our lab used Lipofectamine^{TM} to effectively deliver siRNA to 1321N1 Astrocytoma cells. siRNA delivery and knockdown were quantified using qRT-PCR, and their effect measured by microplate Ca^{2+} assay. The effectiveness of Co_3O_4NPs in a similar system will be tested in this work.

Our goal is to determine if Co_3O_4NPs can safely and effectively deliver β-arrestin siRNA to 1321N1 Astrocytoma cells. To address this goal, we will first determine if Co_3O_4NPs are toxic to these cells. Following toxicity screening, we will investigate whether β-arrestin1 expression is altered in cells that have received Co_3O_4NP-delivered siRNA. Finally, we will determine if Co_3O_4NP-delivery of β-arrestin1 siRNA results in functional changes with respect to $P2Y_2R$ desensitization.

To define toxicity, we will use the MTT (3-(4,5-dimethylthiazol-2-yl)-2,5-diphenyltetrazolium bromide) assay for several concentrations of Co_3O_4NPs. This is a widely used protocol which provides a picture of overall cellular metabolism through conversion of the yellow tetrazolium salt (MTT) into insoluble Formazan, the extent of which is measured

spectroscopically. Absorbance of the supernatant at 570 nm will be compared between wild type (untreated) cells and those that received treatment with Lipofectamine™ or Co_3O_4NPIf cells receiving treatment are not significantly different, the treatment will be deemed non-toxic. If, however, absorbance is significantly lower in treated cells when compared to untreated, the treatment will be considered toxic. Various concentrations of NP will be screened for toxicity to determine concentrations that will be acceptable for testing siRNA delivery.

To investigate the effectiveness of Co_3O_4NPs in delivering siRNA, we will use quantitative RT-PCR (qRT-PCR). Multiple concentrations of Co_3O_4NPs may be used to determine if siRNA effectiveness is dose-dependent, which has been shown in previous trials by Dean (64). Expression of β-arrestin1 in siRNA-treated cells with various delivery methods will be compared to that of untreated cells. If the expression is significantly lower in treated cells, that treatment will be considered successful. Cobalt treatments will also be compared against each other to determine the importance of dosing, with significantly lower levels of expression, and the lack of toxicity as an indication of ideal dose. Cobalt treatments will be compared to Lipofectamine™ treatments, as Lipofectamine™ is an industry standard for delivery of nucleic acids. In each case, significantly lowered expression will be used to define which delivery and dosing methods are successful.

After using qRT-PCR to narrow the Co_3O_4NP dosing range, we will then look at the functional effect of the knockdown by utilizing the well characterized process of $P2Y_2R$ desensitization in these cells. The 1321N1 cell line has been ideal for researching the $P2Y_2$ receptor due to no natural expression of P2 receptors. During the earliest studies, Garrad (1998) describes the stable transfection of wild type and truncated HA-tagged $P2Y_2$ receptors into the cell line, which have since been used for continued studies (43). In 2012, Louiselle designed a

microplate-based Ca^{2+} assay capable of distinguishing nanomolar changes in agonist-dependent $P2Y_2R$ desensitization (68). Each treatment will have 6 replicates, the average will be plotted on a sigmoidal dose-response curve. Two criteria will be used to determine if the treatment is functionally relevant. The EC_{50} of the given treatment must not be significantly different compared to that of untreated cells. This will be an indication that the treatment itself does not affect the activity of the $P2Y_2R$. Additionally, if the IC_{50} is significantly increased, this will indicate the treatment is functionally effective. Finally, cobalt treatment results will be compared to those from Lipofectamine™, with equal or significantly greater IC_{50} as an indication of successful treatment.

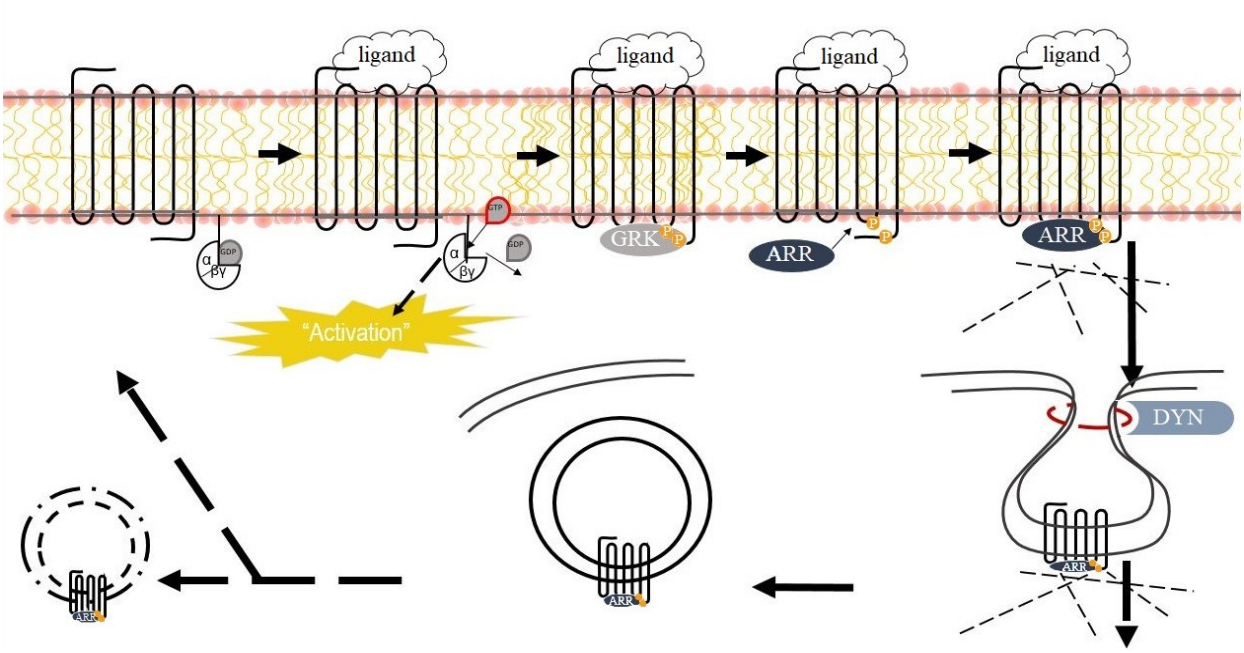

Figure 1. GPCR desensitization and endocytosis. GPCR signal termination follows phosphorylation of the C-terminus of a ligand-bound receptor by GRK, subsequent binding of β-arrestin and internalization through clathrin-mediated endocytosis.

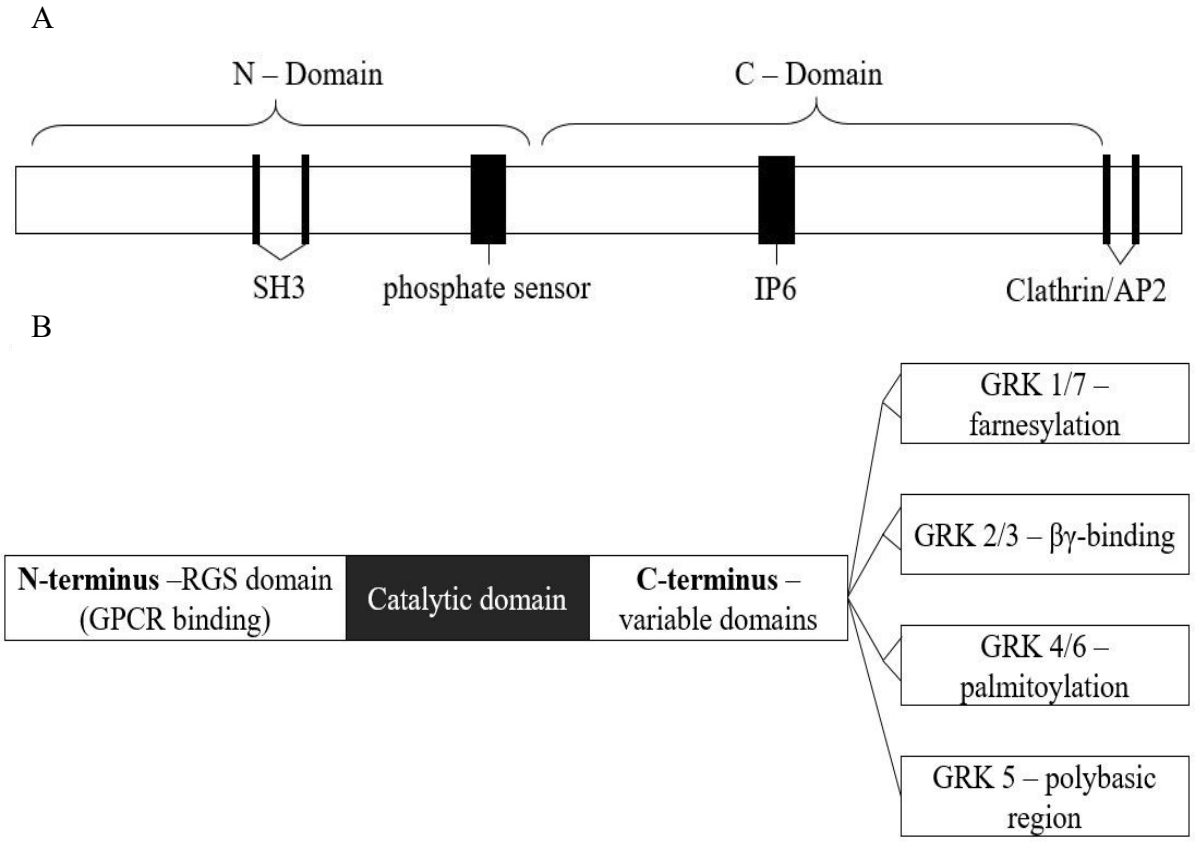

Figure 2. Structure of GRKs and arrestins. A, Graphical depiction of β-arrestin1 and 2 general structure, revised from 'The role of β-arrestins in the termination and transduction of G-protein-coupled receptor signals', Luttrell and Lefkowitz 2002. B, Graphical depiction of GRK protein structure revised from 'Evolving Concepts in G Protein-Coupled Receptor Endocytosis: The Role in Receptor Desensitization and Signaling', Ferguson 2001.

METHODS

Cell Culture

Human astrocytoma cell line 1321N1 was used in all experimentation. For maintenance, cells were grown in an incubator kept at 37 °C, 5% CO_2 and 98% humidity in a 25 cm^2 flask (TPP art iso9001) and cultured twice per week. Briefly, cells were washed with sterile Dulbecco's PBS (Gibco, Gaithersburg, MD) prior to addition of 0.5 ml of 0.25% (v/v) trypsin-EDTA(Gibco) to disrupt adhesion. Dulbecco's Modified Eagles Medium (DMEM, Gibco) supplemented with 5% (v/v) Fetal Bovine Serum (FBS, Atlanta Biologicals), 0.5 mg/ml Geneticin (Gibco) and 1X Antibiotic-Antimycotic (Gibco) was added to the cell suspension to stop trypsin activity, prior to transfer of the desired amount into a new flask. Culture medium was added to bring the volume to 4 ml.

Cobalt Preparation

Cobalt oxide nanoparticles (Co_3O_4NP), provided by Dr. Kartik Ghosh of Missouri State University (Springfield, MO), were prepared in suspensions of 1 mg/ml. Cobalt was massed out and added to a 1.8 ml microcentrifuge tube (Midsci) before adding DEPC-treated (Sigma-Aldrich) Millipore water (Millipore Corporation). The suspension was vortexed on high before sonication in a Fisher Scientific FS20 Ultrasonic Cleaner. Vortexing and sonication was repeated 2 times. The suspension was centrifuged at approximately (16,000 x g) to pellet cobalt. Water was removed by pipetting and the pellet fully resuspended in 70% (v/v) ethanol, using the pipette tip to scrape sedimented cobalt from the side of the tube. The suspension was centrifuged at approximately (16,000 x g) and supernatant removed by pipetting. Cobalt was resuspended in

100% ethanol to bring the final concentration to 1 mg/ml. The Cobalt-ethanol suspension was wrapped in Parafilm and stored at 4 °C until time of use.

For experiments, the cobalt suspension was centrifuged, and ethanol removed by pipette. The pellet was resuspended in DEPC-treated, Millipore water and centrifuged. Water was removed by pipette and the pellet resuspended in water for siRNA (siGENOME SMARTpool, Dharmacon) or Lipofectamine^{TM} (LF, Invitrogen) addition or DMEM for mock treatments. The suspension was then serially diluted to obtain final working concentrations.

Cytotoxicity Screening: Trypan Blue Exclusion Staining and MTT Assay

Cells were grown to 20% confluence in 10 cm^2 dishes prior to administration of Co_3O_4NP in 180, 90, 45, 25 and 12.5 μg/ml treatments. Cells were incubated with Co_3O_4NP treatments for 72 hours prior to staining with Trypan Blue. On the day of staining, Trypan blue was suspended in PBS to yield 0.4% (v/v) solution. DMEM was removed from cells, which were then washed with Hepes buffered saline (HBS). Cells were removed by adding 10 mM EDTA in HBS and placing on a rocker for 1 hour, turning plates ¼-turn every 15 minutes. Using a p-1000 micropipette, the suspension was pipetted up-and-down directly over the cells to break adhesions and fully suspend in the solution. The entire suspension was transferred to a 2 ml microcentrifuge tube and Trypan stain added for final concentration of 0.2%. The suspension was pipetted to mix before a small volume was added to a hemocytometer and counted through the microscope. All cells were counted to compare the number of cells stained blue to those unstained.

The MTT assay was used to determine cellular metabolism as a measure of the toxicity of Cobalt treatments. Cells were seeded overnight in a clear, 24-well plate (NUNC, Nunclon

surface) at 20% confluence. On the following day, cells were left untreated or treated by column with hygromycin 800 µg/ml, Co_3O_4NP at 180 or 12.5 µg/ml, or Lipofectamine™.

Cells were incubated in indicator-free, antibiotic-free Optimem medium supplemented with 5% FBS and the various treatments for 72 hours prior to the assay. On the day of the assay, MTT suspension was prepared with slight adjustments to the manufacturer's instructions, 7.5 mg MTT (Invitrogen) was massed out and added to 1.5 ml PBS and vortexed until dissolved. Cell culture medium was removed and replaced with fresh, serum-free, antibiotic-free medium and MTT suspension added to each well for final concentration of 1 mM. The plate was wrapped in foil and incubated at 37 °C for 4 hours. After incubation, 10% (w/v) SDS (Fisher Scientific) in 0.01 M HCl was added to the cells, mixed by pipetting and incubated at 37 °C for 4 hours. After final incubation each well was mixed thoroughly, and the absorbance measured at 570 nm using the SpectraMax Paradigm plate-reader. All data from 'Blank' replicates was averaged and subtracted from each well. Each blank-subtracted absorbance value was plotted onto a bar graph showing error bars indicating SEM. One-way ANOVA was used to determine significance, p-values were indicated with asterisks (*).

qRT-PCR

Cells were cultured overnight in antibiotic-free, reduced-serum media supplemented with 5% (v/v) FBS, using in 10 cm^2 dishes (Falcon) to yield 20% confluence. On the day of transfection, medium was removed, and cells washed in sterile PBS and replaced with serum-free, antibiotic-free Optimem medium.

Co_3O_4NP dilutions were prepared and resuspended in RNase-free water. Treatments were prepared in aggregate so that 12.5 µl of 20 µM siRNA per well was added to each cobalt dilution

and the suspension was immediately centrifuged for 7 minutes to pellet and complex RNA-Co_3O_4NP. Supernatant was removed and the remaining pellet resuspended in serum-free, antibiotic-free medium and added directly to the cells in 200 µl volumes to yield final in-well cobalt concentrations of 25, 45, 90 and 180 µg/ml. Cells were stored in a 37 °C incubator for 72 hours prior to harvesting RNA.

On the day of RNA isolation, medium was removed from the cells and 400 µl of TRIzol Reagent (Sigma-Aldrich) added directly to the dish. The TRIzol was left on cells for several minutes to ensure complete removal from the dish, cells were then transferred into a microcentrifuge tube where 80 µl of ice-cold chloroform was added and mixed by inversion. Tubes were then centrifuged at approximately (16,000 x g) at 4 °C for 15 minutes and the resulting aqueous layer was transferred to a new tube. To the new tube, 200 µl of 100% isopropanol was added and mixed by pipetting before storing at 4 °C overnight to maximize precipitation. The next day, tubes were centrifuged at approximately (16,000 x g) in 4 °C to pellet RNA. Supernatant was removed and 400 µl of 75% (v/v) ethanol added to wash the pellet. Suspension was centrifuged and supernatant removed with a pipettor. To fully dry the RNA pellet, tubes were left open until all ethanol had evaporated, prior to resuspension in 50 µl RNase-free water. RNA was quantified immediately using Nanodrop 2000 (Thermo Fisher Scientific) and stored at -80 °C until cDNA synthesis.

Thermoscript^{TM} RT-PCR System was used with minor adjustments to manufacturer's instructions for cDNA synthesis. To begin, provided oligoDT, dNTPs and water were prepared together and aliquoted for each individual reaction prior to addition of RNA template. Varying volumes of RNA were added so that each reaction contained the same final concentration of RNA template. This reaction was heated to 65 °C in the thermal cycler (PTC-200, MJ Research)

and transferred onto ice. A cDNA master mix of 4 µl of 5X buffer, 1 µl of 0.1 M DTT, 1 µl of RNaseOUT, 1 µl (15 U) or Thermoscript-RT, and 1 µl of water per reaction was prepared in aggregate and 8 µl added to each primed reaction. The samples were added to the thermal cycler for the following protocol: 45 minutes at 55 °C, 5 minutes at 85 °C. Next, 1 µl of RNase H provided in the kit was added to each reaction and incubated at 37 °C for 20 minutes. Resulting cDNA was stored at -20 °C until use in quantitative PCR.

For quantitative PCR, a master mix of SsoFast EvaGreen Supermix (Bio-Rad), primers (Table 1, IDT), and water was prepared and added in 18 µl aliquots to a 96-well plate (Bio-Rad). Two µl of cDNA template was added to the desired wells. The plate was added to the thermal cycler (Bio-Rad CFX Connect Real Time System) and after 2 minutes at 98 °C for initial melting, 50 cycles of 98 °C for 5 seconds, 60 °C for 30 seconds. Finally, melt peak analysis was performed starting at 54 °C and increasing 0.5 °C every 10 seconds up to 98 °C. Serial dilutions of 0.1, 10 and 100 µg of genomic DNA were included for construction of a standard curve and starting quantities calculated by the software were used to determine fold-change in expression. All replicates were normalized to housekeeping gene GAPDH by dividing by the average starting quantity and then compared to untreated cells to determine fold-change.

Microplate Calcium Assay

Cells were seeded in serum-free, antibiotic-free Optimem overnight in a clear-bottom 96-well plate (BRANDplates, Germany) the day before transfection. Transfected cells were used for calcium assays 48 hours after siRNA application. A FLUO4 Calcium assay kit (Molecular Probes) was used with modifications to the manufacturer's instructions. The buffer provided in the kit consisted of 1x HBSS and 20 mM HEPES and was supplemented with 0.5% BSA (Fisher

Scientific) on the day of the assay, hereafter called HBSS+. Probenecid provided in the kit was resuspended in 1 ml of assay buffer and divided into 100 µl aliquots. On the day of the assay, one bottle of dye was resuspended in 10 ml HBSS+ and 100 µl Probenecid, which prevents extrusion of the dye from cells, was added before mixing thoroughly by vortex for several minutes. Each well was washed with 100 µl HBSS+ prior to addition of 100 µl dye-solution in all but the top and bottom rows, which served as blanks. Cells were incubated with dye for 40 minutes at 37 °C. During this incubation, the microplate reader was warmed to 37 C. UTP was prepared by serial dilution in pre-warmed HBSS+ for of 3 ml of each activation concentration, 10^{-3} M, 10^{-4} M, 10^{-5} M, 10^{-6} M, 10^{-7} M and 10^{-8} M, and 6 ml of 4 X 10^{-6} M for re-challenge. Additionally, during this incubation time the microplate reader (FLUOstar Optima, BMG Labtech) was pre-warmed to 37 °C and UTP primed for injection. The injection reservoirs were rinsed by priming and back flushing with 1 ml of DI water, prior to priming with 1 ml of starting activation concentration, 10^{-8} M UTP with injection needle 1, and 4 X 10^{-6} M with injection needle 2 for re-challenge. After incubation, the plate was inserted into the microplate reader, FLUO4-DESENS protocol was selected and fluorescence measured for 3 seconds to obtain a baseline prior to challenge with UTP from injection needle 1, and measurement for 19 seconds to determine response. The protocol was set to take all measurements of the same concentration within 5 minutes. Similarly, FLUO4-RECHALL protocol was selected to perform the same procedure on cells previously challenged with an activation concentration of UTP, using injection needle 2 for delivery of UTP. Both protocols were carried out, one after another for each concentration of UTP. Blanks were averaged for each activation concentration of UTP and used to normalize fluorescence data collected. For each well, normalized average baseline fluorescence was calculated and subtracted from the maximum post-UTP fluorescence.

Fluorescence change for each well was used to create a sigmoidal dose-response curve in GraphPad for both activation and re-challenge. SEM is represented by error bars for each point.

Table 1: Primers used for qRT-PCR analysis of β-arrestin1 expression

Primer Name	Sequence	Location (bases)	cDNA (bp)	gDNA (bp)
Isoform Differential	F-ACGAACTTGGCCTCTAGCAC R-TGGCGAGCAAAGTCCTCAAA	82,730 to 98706	266/290	7,858
‘P1”	F-AAAGGGACCCGAGTGTTCAAG R-CGTCACATAGACTCTCCGCT	5,228 to 73,354	159	68,126
“P2”	F-CCTGACCTTTCGCAAGGACC R-CAAGCCTTCCCCGTGTCTTC	73,401 to 75,689	204	2,288
“P3”	F-GCTTGCGGTGTGGACTATGAA R-CTGGGGCATACTGAACCTTCC	75,684 to 78,126	112	2,442

RESULTS

Cytotoxicity of Cobalt Oxide Nanoparticles

Cytotoxicity screening was initially attempted using Trypan blue exclusion staining. This method was unsuccessful due to difficulty in distinguishing stained cells from those containing cobalt nanoparticles. For this reason, it was determined that an assay measuring metabolic activity may provide a clearer representation of the cytotoxicity of cobalt oxide nanoparticles.

The employed MTT assay relies on intracellular reduction of a yellow/clear MTT (represented in Fig. 3 'Blank' column) to the insoluble, dark blue/violet formazan salt. Lower absorbance occurs with less reduction of MTT, presumably a consequence of depressed metabolic activity, resultant from fewer living, healthy cells. After 72 hours of incubation with various treatments, spectroscopic analysis is used to show MTT metabolism. Hygromycin treatment was chosen as a positive control for cell damage. After 4 hours incubation with MTT and the addition of SDS/HCl to solubilize formazan, there was an immediately visible difference in color of the cell-free and Hygromycin treated columns when compared to DMEM, Lipofectamine^{TM} and Co3O4NP treatment. At the end of the full incubation time, wells containing cobalt, Lipofectamine^{TM}, and mock treatments were visibly dark blue/purple while the control and hygromycin wells remained yellow (Fig. 3A). MTT metabolism was significantly diminished ($p < 0.05$) in Hygromycin trials compared to all others. There was no significant difference in absorbance between cells treated with cobalt, Lipofectamine^{TM}, or mock treatments; indicating that the delivery method has minimal effect on cell viability (Fig. 3B). Previous trials by Dean revealed a dose-dependent pattern of effectiveness for Co_3O_4NP to deliver effective splice-switching oligomers to A375 pLuc reporter cells (64). Here, higher

concentrations of Co_3O_4NP were included in subsequent experiments due to lack of any measurable toxicity and the potential for greater efficacy.

Expression Analysis by qRT-PCR

β-arrestin1 expression was quantified through qRT-PCR to determine the effect of treatment with siRNA delivered by Lipofectamine™ or Co_3O_4NP. First, primers were optimized through amplification with GoTaq polymerase at 4 different temperatures each, determined by manufacturer recommendations (Fig. 4). Amplification using 4 different sets of primers was tested on genomic DNA and cDNA. The differential primer amplifies both β-arrestin isoforms, differing by 24 bases. The differential primer set amplified genomic DNA most efficiently at 55 °C and cDNA at 59 °C, with substantial primer dimers present in all temperatures tested. P1 primer set shows equivalent amplification of cDNA at each temperature trialed, with no apparent amplification of genomic templates (Fig. 4A). P2 primers amplify cDNA with greatest efficiency at 57 °C, while gDNA is amplified more efficiently at each temperature tested. P3 primers amplify cDNA with the least primer dimers at 59 °C, where amplification of gDNA is least efficient (Fig. 4B). Due to preferential cDNA amplification efficiency, the "P2" primer set was chosen for expression analysis of β-arrestin via qPCR.

Notably, the "Isoform Differential" primer set allowed for clear distinction between the 260 bp and 290 bp β-arrestin isoforms. Optimal amplification of each occurs when using an annealing temperature of 59 °C, which also corresponds to the least efficient amplification of genomic DNA, a fragment >8,000 bp.

Next, the P2 primer set was used in qRT-PCR to quantify β-arrestin1 expression and the level of knockdown in transfected cells. For each experiment, extracted RNA was quantified by

spectrophotometric analysis and the same mass (in ng) was used to create cDNA from each treatment type. During qPCR each sample was run in triplicate. Each primer set was shown to have a unique amplification pattern with respect to cycle threshold and reaction plateau (Fig. 5A). The melt peaks for GAPDH, β-arrestin1 and standard melt temperatures were 81.5-82, 86-86.5 and 81.5 °C, respectively, and show little variation between treatment types and replicates, indicating no contamination, and selective amplification of the desired products (Fig. 5B). For quantification, 1, 10 and 100 ng of gDNA were used to create a standard curve (Fig. 5C). As with all other samples, standards were run in triplicate. In the standard curve, $R^2 = 0.999$ indicates that any differences in amplicon starting quantity between samples were due to actual differences in expression.

Analysis of the qRT-PCR data and extrapolation of β-arrestin1 expression level started by calculating the 'normalized starting quantity' for replicates of each sample from 4 separate experiments. Starting quantity (Sq) of individual β-arrestin1 wells were divided by the GAPDH average Sq per sample to produce normalized β-arrestin1 starting quantities, or ΔSq. Next, the average ΔSq from untreated, and vehicle treatments ('Wild Type', 'Lipofectamine™', 'Co_3O_4NP', all (-) siRNA) was set to '1' and all individual ΔSqs from that experiment were compared to this value to produce ΔΔSq, a normalized change in expression relative to treatment type. Data from each of four experiments have been compiled (Appendix A, B, C, D) and depicted graphically (Fig. 6, Appendix E).

Cells that did not receive siRNA ('Wild Type', 'Lipofectamine™', 'Co_3O_4NP') were used as a standard for β-arrestin1 expression, all treatments were compared to this value. Cells treated with either Lipofectamine™ or Co_3O_4NP but no siRNA (Vehicles, (-) siRNA) were included to control for interference from these delivery agents; both were expected to have the

same β-arrestin1 expression as untreated cells. Though there were no significant differences between the wild type and vehicle treatments, there was too much variation in C_t and subsequent calculations that no reliable baseline of β-arrestin1 expression could be determined.

This experiment was designed to test how effectively Lipofectamine™ and Co_3O_4NP deliver siRNA to knockdown β-arrestin1 expression. All trials with siRNA were expected to show a knockdown in β-arrestin1 expression, with a dose-dependent pattern from Co_3O_4NP and a possible plateau of effectiveness. However, there are no significant differences in relative expression of β-arrestin1 across all treatment types (Fig. 6A). Notably, Lipofectamine™ delivery of siRNA also showed no significant reduction in β-arrestin1 expression, despite previous success (68). Overall, each cDNA appears to show some degree of knockdown with siRNA treatments, however, each also contains unexpected results, and again, too much variation to delineate any statistically significant trends (Fig 6B). All but cDNA 4 showed instances of β-arrestin1 overexpression, including points from each showing a 2-fold induction. Notably, normalization of cDNA 4 samples reveals that β-arrestin1 mRNA was present in much lower starting quantities in these samples compared to all others, such that it was not visible on a graph with the other 3 experiments of ΔSq data (normalized, not relative).

When no significant pattern of relative β-arrestin1 expression could be identified across experiments, it became important to try to determine the nature of the discrepancy. To assess the quality of current GAPDH data as a reference for normalization of β-arrestin1 expression, Appendix E was constructed using Cycle threshold (C_t) values from all cDNA sets. This C_t value represents the first cycle at which detectable products are made in direct proportion to the starting quantity of the template and is used in the program's calculation of Sq. In general, a lower C_t is associated with greater starting quantities, though experimentally the exact nature of

this relationship is dependent on the primer-template interaction throughout a cycle, known as primer efficiency. On average, GAPDH templates reached a detectable range nearly 10 cycles before β-arrestin1 templates (Appendix A), such that the graph is visibly split into 2 hemispheres (Appendix E). The least variation between GAPDH replicates is seen during experiments cDNA 2 and 4, though no predictable GAPDH level could be determined and none of these results are statistically significant.

Functional Consequences of β-arrestin1 Knockdown: Ca^{2+} Assays

Our lab recently developed a microplate-based calcium assay which was used to determine the functional consequences on $P2Y_2$ receptor activity following β-arrestin1 knockdown by siRNA treatments. Presently, the results of siRNA delivered by industry standard Lipofectamine™ are compared to that delivered by Co_3O_4NP to determine the efficiency of this new method for nucleic acid delivery. Since the experiment was designed to test the knockdown of β-arrestin1, a protein involved in termination of GPCR signaling, there should be no significant difference in activation responses between any of the treatments, including those which received siRNA. In all trials, there is a dose-dependent response to increasing concentrations of UTP (Fig. 7, Appendix F). EC_{50} (M) values of untreated, LF vehicle, LF + siRNA, Co_3O_4NP Vehicle, and Co_3O_4NP + siRNA are 4.697×10^{-6} 6.997×10^{-7}, 4.240×10^{-7}, 6.11×10^{-6}, and 3.491×10^{-6}, respectively. One-way ANOVA performed within the GraphPad Prism software reveals no significant differences between any treatment type.

Five minutes after the initial activating dose of UTP, a secondary, re-challenging dose of 4×10^{-6} M UTP was administered (Fig. 8, Appendix G). During desensitization, effective knockdown with siRNA will be determined by comparing the overall shape of sigmoidal dose-

response curves, and IC_{50} values of all treatments. Using the Wild Type IC_{50} as a standard, 'effective knockdown' will be indicated by an increase in the IC_{50}, which may also be visible on the graph as an upward and/or rightward shift in the curve. Lipofectamine^{TM} and Co_3O_4NP vehicle treatments (no siRNA) should be comparable to Wild Type with no significant differences in IC_{50}. Any treatment receiving siRNA should reveal some functional consequences indicative of knockdown, and greater doses of Co_3O_4NP should be associated with more effective knockdown. All trials exhibited some decline in their ability to respond to this re-challenge around 5x 10^{-6} M UTP and complete inhibition when initial UTP doses were sufficiently high (1 to 5x 10^{-4} M UTP). Treatment types are compared directly by calculation of IC_{50}, which is the initial ligand concentration sufficient to prevent 50% response upon re-challenge. IC_{50} (M) for untreated, LF Vehicle, LF + siRNA, Co3O4NP Vehicle, and Co3O4NP + siRNA are 2.232x 10^{-8}, 1.143x 10^{-6}, 6.738x 10^{-7}, 4.265x 10^{-6}, and 4.827x 10^{-6}, respectively. One-way ANOVA performed within the GraphPad Prism software reveals no significant difference between any treatment types.

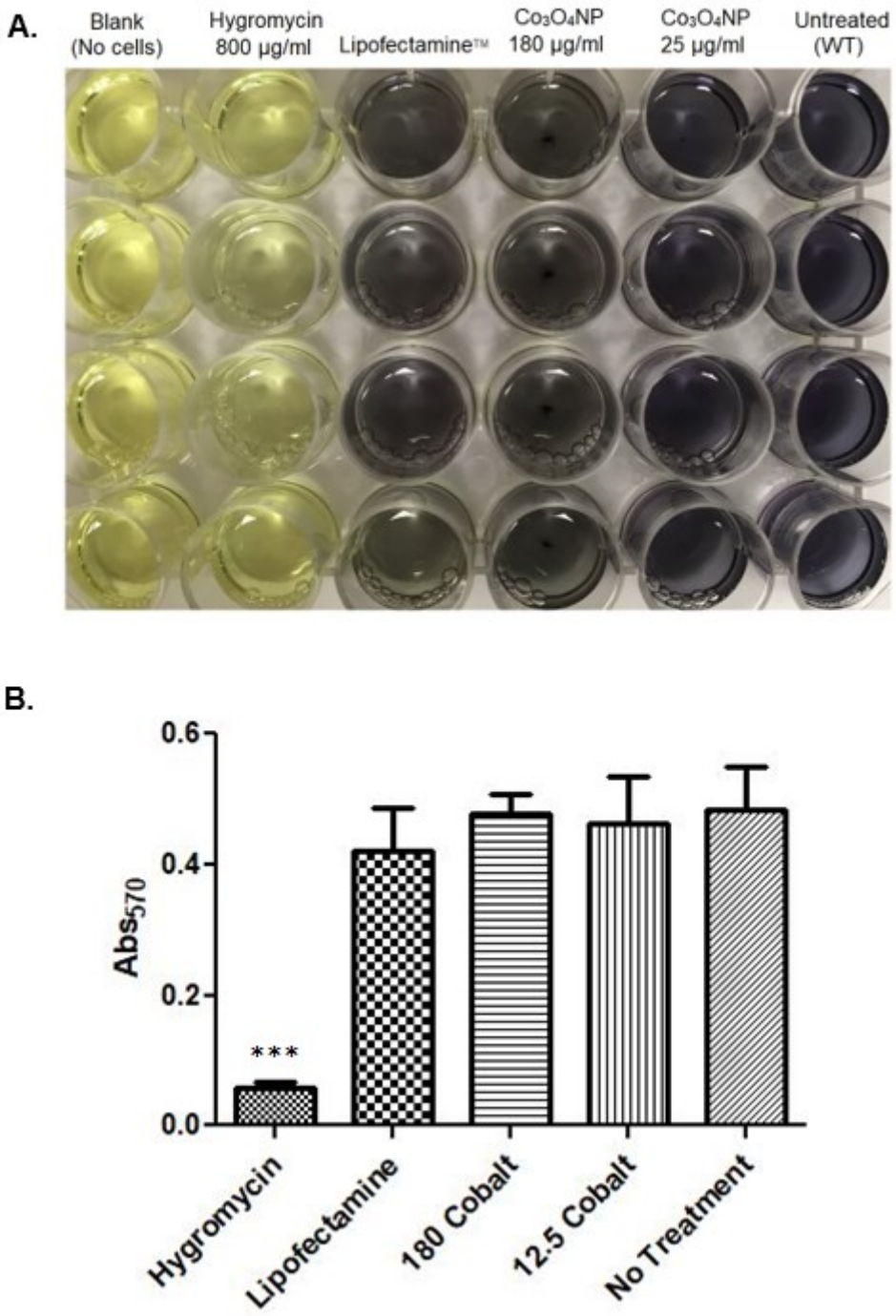

Figure 3. MTT Metabolism following 72-hour treatments. Metabolism of MTT in cells treated for 72 hours with hygromycin, Lipofectamine, cobalt oxide nanoparticles, or media only. A, Visible differences in MTT metabolism. B, A_{570} readings collected from SpectraMax Paradigm Spectrophotometer and analyzed using GraphPad Prism 8. Cell-free (blank) average was subtracted from all other measurements to produce blank-corrected data. *** $p<0.05$, n=4.

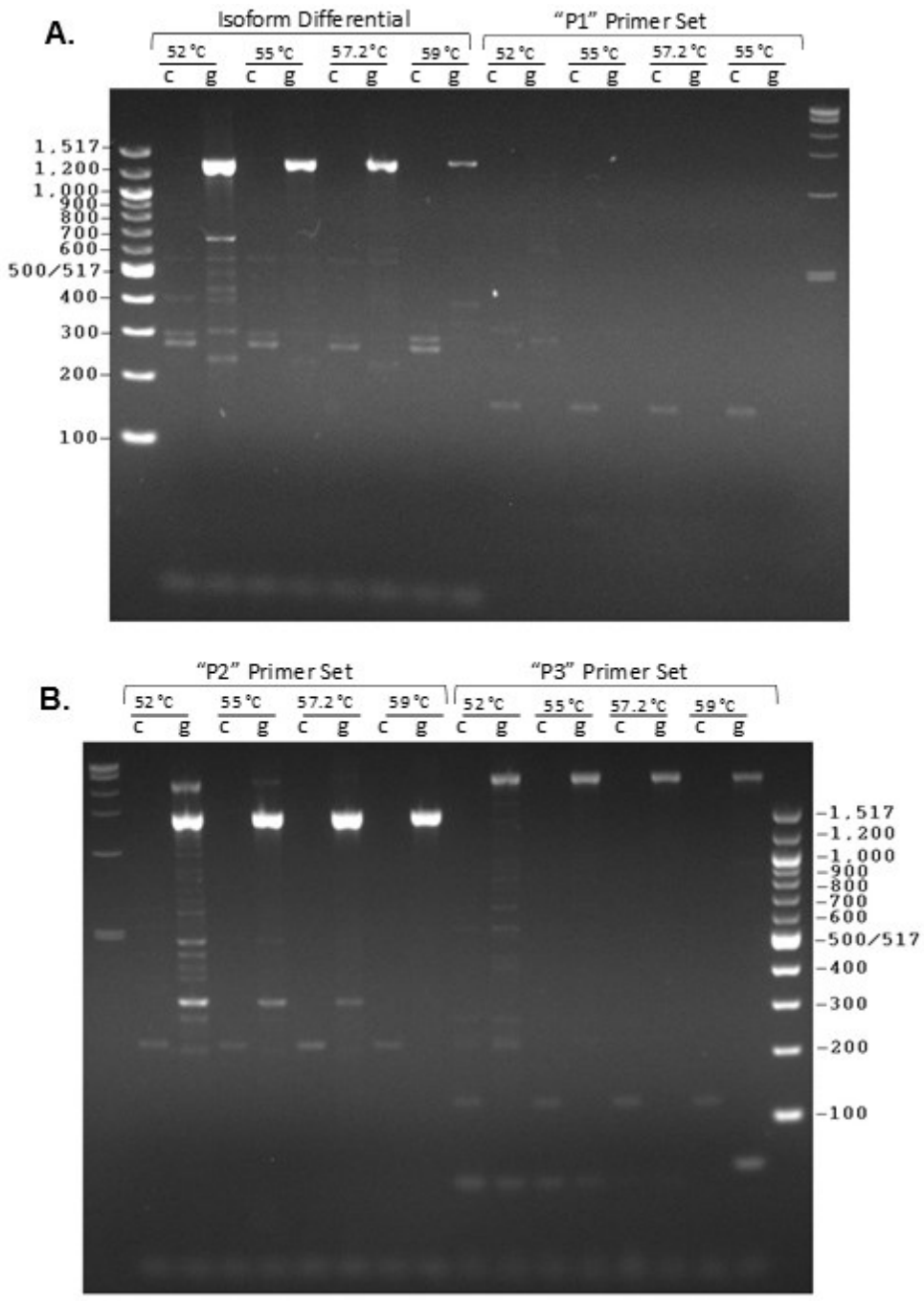

Figure 4. Optimization of qPCR primers with GoTaq Green. Optimization of 4 new sets of primers for amplification of β-arrestin using GoTaq Green. 'c' is used to indicate cDNA templates, and 'g' for gDNA templates. A, "Isoform Differential" primers allow for the distinction between both β-arrestin isoforms (266, 290 base pairs) and the Genomic DNA (7,858 bp). "P1" primer set shows of cDNA (159 bp) at each temperature, with no apparent amplification of genomic templates (68,126 bp). B, "P2" primers amplify cDNA (204 bp) and gDNA (2,288 bp). "P3" primers amplify cDNA (112 bp) and gDNA (2,422 bp).

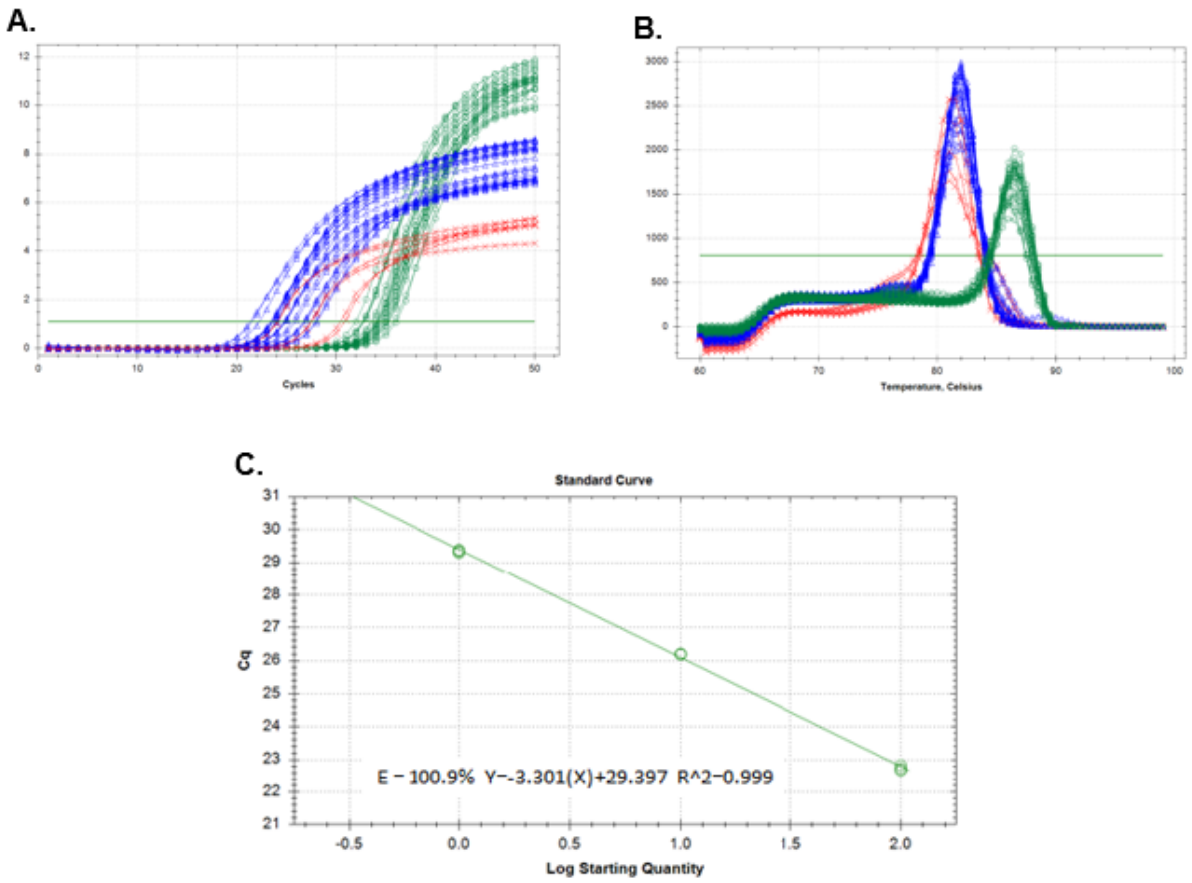

Figure 5. Amplification, melt peak, and standard curve. Quantification of β-Arrestin1 expression in siRNA, mock and untreated cells. A, Amplification curves of GAPDH (blue), Arrestin (green) and standards (red) per cycle of qRT-PCR. B, Melt peaks of GAPDH (blue), Arrestin (green) and standards (red) qRT-PCR products after 50 cycles. C, Standard curve produced by the software used to calculate starting quantities (Sq) of unknown samples.

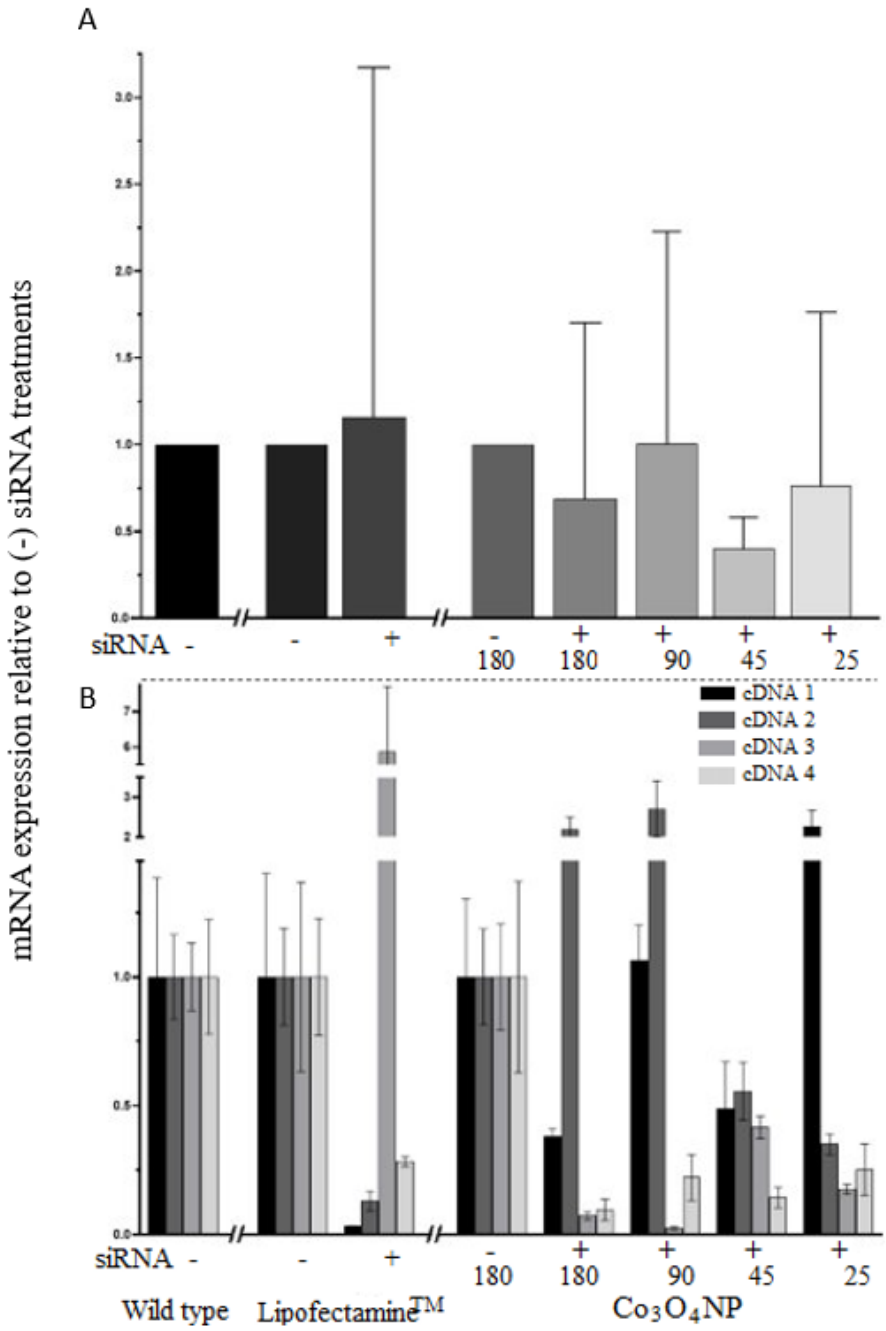

Figure 6. Normalized β-arrestin1 expression relative to treatment type. The 'Standard' function integrated in the thermocycler software reported a starting quantity (Sq) for 3 replicates of each treatment. Each Sq was compared to an average GAPDH Sq to report ΔSq, a normalized β-Arrestin1 expression level. ΔSq from cells grown in DMEM with no additional treatment, or vehicle-only/no siRNA ('Wild Type', 'Lipofectamine', 'Co_3O_4NP' was set to '1' and all other values from the treatment set compared to this as ΔΔSq, the relative 'change-over-baseline' expression for each individual treatment. A, Compiled data from 4 separate experiments. B, 4 experiments shown separately.

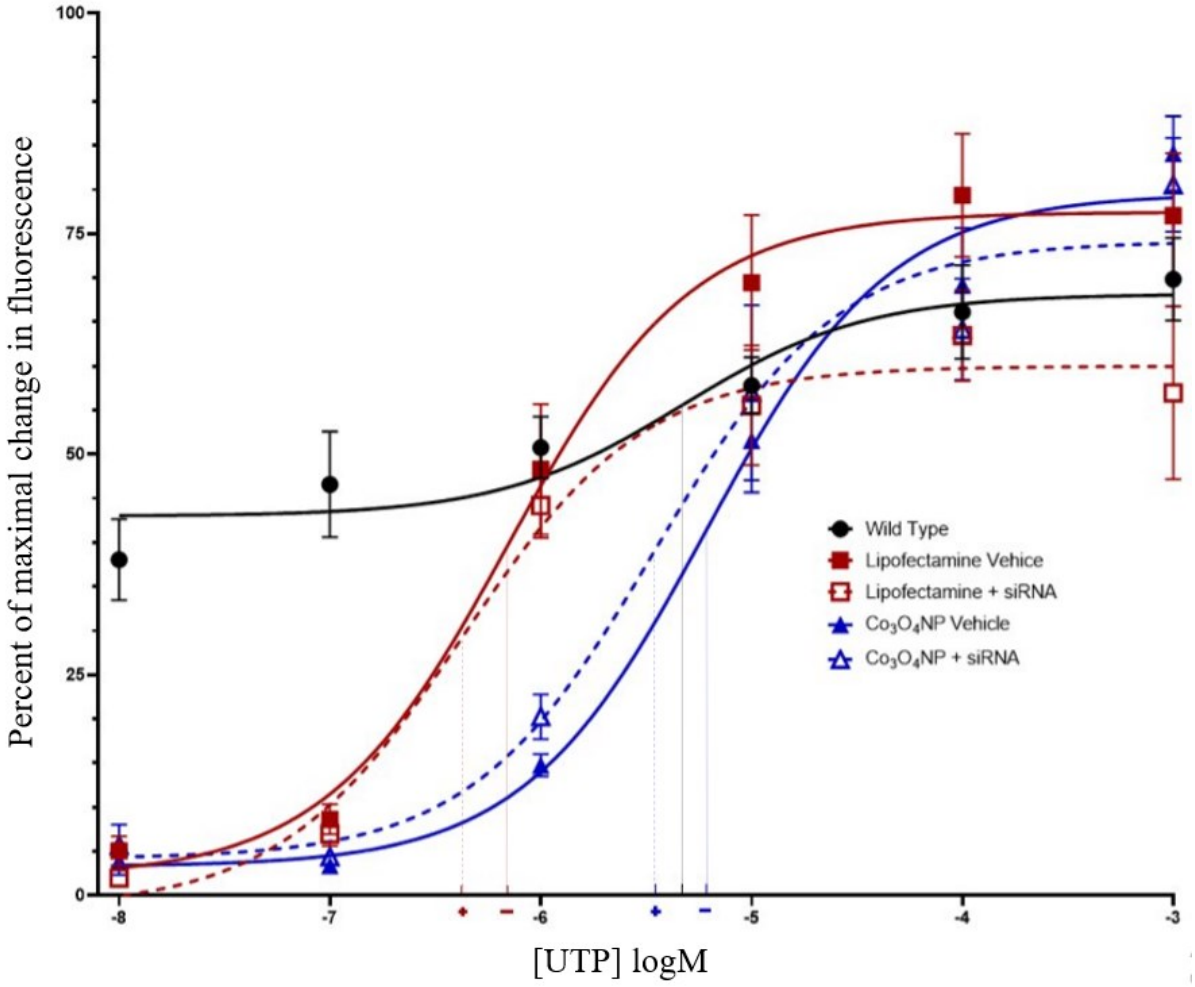

Figure 7. Activation of P2Y$_2$ R by UTP in 1321N1 astrocytoma cells. P2Y$_2$R Ca^{2+} response to varying concentrations of UTP. Cells were grown in a 96-well plate for 24 hours prior to treatment with vehicle, or ARRB1-siRNA delivered by LF or Co_3O_4NP. Intracellular changes in Ca^{2+} are measured by changes in fluorescence from Ca^{2+}-binding dye Fluo4-NW. GraphPad Prizm 8 was used to produce sigmoidal dose-response graphs comprised of 6-replicates for each treatment. EC_{50} for LF Vehicle, LF + siRNA, Co_3O_4NP Vehicle, and Co_3O_4NP + siRNA are 6.997×10^{-7}, 4.240×10^{-7}, 6.11×10^{-6}, and 3.491×10^{-6}, respectively. The program was also used to perform a one-way ANOVA which reported no significant difference between the treatment types (p=0.5323).

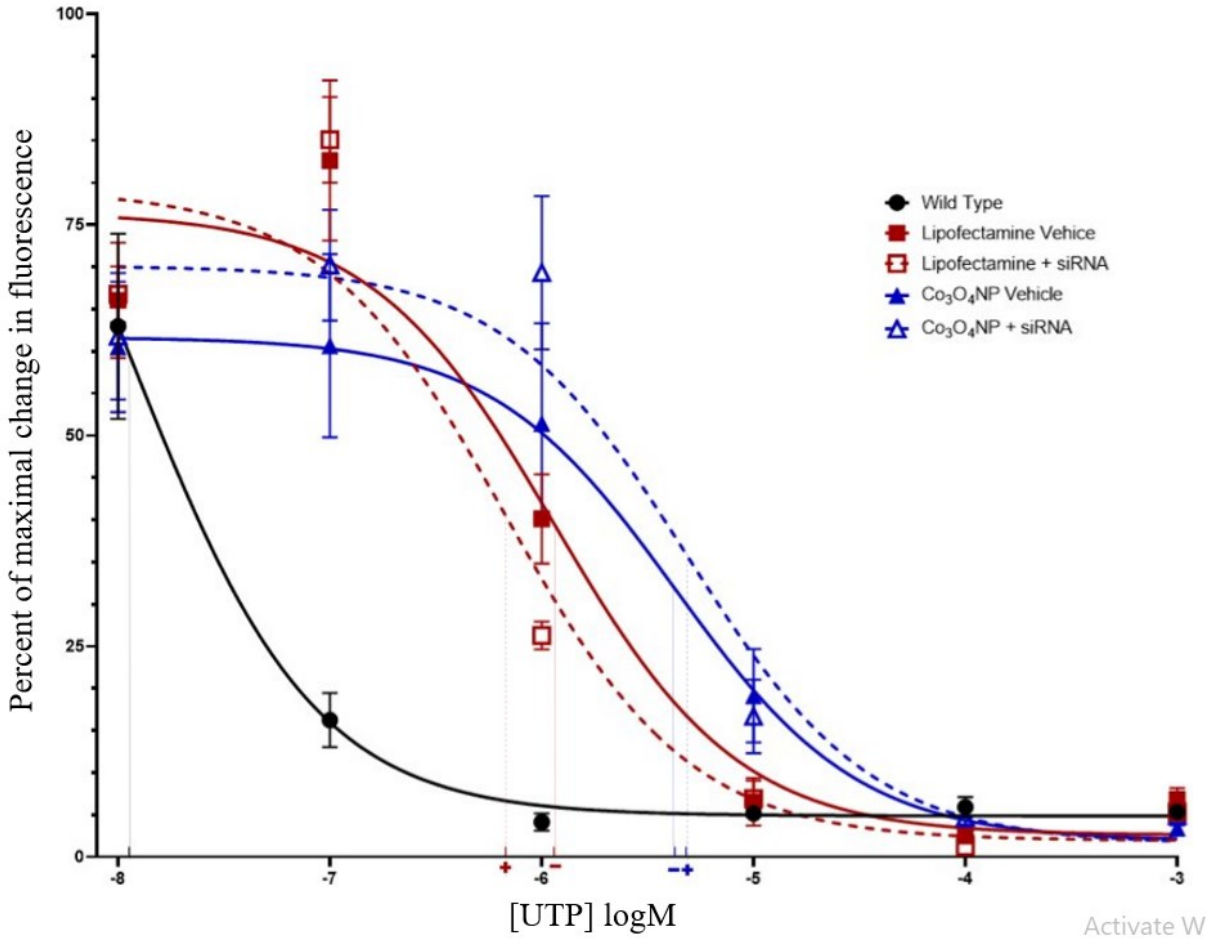

Figure 8. Desensitization of $P2Y_2$ R in 1321N1 astrocytoma cells after prolonged exposure and re-challenge by UTP. $P2Y_2R$ Ca^{2+} response to re-challenge by $4e^{-6}$ M UTP. Cells were grown in a 96-well plate for 24 hours prior to treatment with vehicle, or ARRB1-siRNA delivered by LF or Co_3O_4NP. Resulting intracellular changes in Ca^{2+} are measured by changes in fluorescence from Ca^{2+}-binding dye Fluo4-NW. 5 minutes after an initial dose of UTP, cells were re-challenged with $4e^{-6}$M UTP. Resultant Ca^{2+} changes are inversely related to initial [UTP], with no secondary response after incubation under 1×10^{-4} to 5×10^{-4} M UTP, dependent upon treatment. GraphPad Prizm 8 was used to produce sigmoidal dose-response graphs comprised of 6-replicates for each treatment. IC_{50} for LF Vehicle, LF + siRNA, Co_3O_4NP Vehicle, and Co_3O_4NP + siRNA are 1.143×10^{-6}, 6.738×10^{-7}, $4{,}265 \times 10^{-6}$, and 4.827×10^{-6}, respectively. One-way ANOVA reported no significant difference between treatment types ($p = 0.1661$).

DISCUSSION

Cytotoxicity of Cobalt Oxide Nanoparticles

Toxicity screening was the first indication that working with Co_3O_4NP would not be entirely straight forward. Using Trypan-Blue exclusion staining proved ineffective due to difficulty distinguishing between stained cells and those with internalized cobalt. The increased time required to perform the test resulted in more stained cells, as the screen is time-sensitive, these results did not appear to be indicative of actual cell health.

Initial trials with the MTT assay began in 0.3 cm^2 wells/96-well plate. No change in absorbance was noted between control cells and those exposed to 180 µg/ml cobalt. After this, doses up to 500 µg/ml were used, which led to conflicting results: the absorbance increased proportionally to increases in cobalt concentrations. Rather than MTT metabolism, it seemed that absorbance was increased due to cobalt sediments blocking the sensor under the well. To account for this, 2 cm^2 (24-well) plates were used, in addition to a centrifugation step following the final incubation prior to taking the reading. A read area was selected around the perimeter of the well and measurements were taken avoiding the sediments of cobalt in the center. These trials have indicated that none of the cobalt treatments induced cytotoxic effects, however more diverse trials may still be required.

Previous research by Chattopadhyay *et al* indicated that Co_3O_4NP with phosphonomethyliminodiacetic acid (PMIDA) exhibited selective toxicity toward cancer cells. This was determined in a study comparing cytotoxicity of varying doses of doxorubicin, a cell-cycle specific chemotherapeutic that inhibits topoisomerase II, to that of PMIDA-coated Co_3O_4NP in primary lymphocyte and oral squamous cells from patient samples, and Jurkat and KB cancer cell lines. The research indicated that doses of 25 µg/ml PMIDA-Co_3O_4NP had no

apparent effect on the primary cells, while inducing significant toxicity in the cancerous cell lines, diminishing viability by about 60% compared to the control (70).

Expression Analysis by qRT-PCR

Initially, the same β-arrestin1 primers used in the study by Louiselle were employed, however it became apparent that an undefined contaminant was the only measurable product, this was confirmed by agarose gel electrophoresis, using samples directly from the wells following the qPCR procedure (data not shown). This product cannot be explained as the cDNA or gDNA β-arrestin1 amplicon, nor is it the result of primer dimers. This product dominated every well, including those with no template. Following this discovery the issue was resolved by ordering entirely new primers, 3 sets directly from the Harvard Primer database (PrimerBank IDs 320461704c1, 320461704c2, and 320461704c3) (71–73) and one set designed to differentiate the isoforms of β-arrestin.

'Isoform differential' primers were designed to delineate expression discrepancies between β-Arrestin isoforms 1 and 2, which differ by excision status of a single intron, 8 amino acids (24 bases) in length. Though these primers could not be useful in expression analysis via qPCR due to the likelihood for variation in amplification efficiency of each individual product, they may still be beneficial in later studies. Research has shown that the two isoforms may contribute opposing regulatory effects on receptor tyrosine kinases such as insulin-like growth factor type 1 receptor (IGF-1R), with β-arrestin1 binding preferentially to ligand-occupied receptor to potentiate MEK/ERK signaling, while β-arrestin2 has a propensity for binding unoccupied IGF-1R to initiate ubiquitination of the inactivated receptor (74). Investigating

expression differences of the two isoforms has the potential for use as a cancer marker for screening, or even a target for treatment in the future.

Lack of amplification of genomic DNA using the "P1" primer set as seen in Fig. 4A may be due to the design of the primer flanking multiple introns, the predicted product of which exceeded 60,000 base pairs.

Analyzing the results of qPCR posed a major difficulty as small changes in methods resulted in major discrepancies in measured expression of β-arrestin1. Analyzing individual data sets from RNA isolated on separate dates, there are no statistically significant trends which would indicate successful knockdown of β-arrestin1. However, these data are not sufficient to conclude that Co_3O_4NP are unable to safely deliver functional siRNA. Since Lipofectamine™ has previously been shown to successfully deliver functional siRNA for detectable knockdown (Louiselle), these treatments served as an internal control. Had every part of the experiment gone as planned, there should have been knockdown in the LF-RNA treatments. Since there was none, the rest of the qRT-PCR data also falls under suspicion.

GAPDH was used as a reference gene due to previous success and readily available primers. One vital assumption for the analysis of qPCR-derived expression data is that the reference gene be present in stable levels, regardless of any treatments. There should be no significant difference in expression of this reference gene between samples in the same experiment, and ideally, very little difference from one experiment to another. If too much variation occurs with reference expression, whether linked to treatments or not, the whole analysis becomes unreliable due to the potential for magnification of discrepancies upon extrapolation. Within each experiment, some GAPDH C_Ts resulted in a large range of several hundred between SQs. This finding brings into question the validity of the normalization

calculation and challenges confidence in the final values reported. It is possible that the experimental treatments affected GAPDH expression, however, variation between replicates indicate further trials are required. Since RNA extractions were quantified, and a specific total mass was chosen prior to cDNA synthesis, differences in product quantity during qPCR should relate to overall expression, rather than input.

Despite obvious shortcomings, one thing may be ascertained from the data presented here; β-arrestin1 transcripts are present inside these cells at far lower quantities than the chosen reference gene, GAPDH. This may also complicate extrapolation and analysis since the comparative β-arrestin1 presence is diminutive, with average normalized β-arrestin1 SQ about 0.005 across all data sets – 0.5% compared to cellular GAPDH presence. This was not entirely unexpected, as initial trials were designed to complete only 40 cycles, which, for the β-arrestin1 template was not sufficient to bring the reaction into the canonical 'plateau phase', where various reactants begin to reach depletion and the quantity of product following each cycle is increasingly unlikely to reflect starting quantities.

Functional Consequences of β-arrestin1 Knockdown: Ca^{2+} Assays

Data retrieved from calcium assays leaves much to be desired for reliability, as indicated by variations between multiple trials. To some degree, this may be accounted for with the microplate reader used. The expectation was that the microplate reader would be simple to set-up for use in these assays, however multiple times the machine needed significant modifications before use. Near the beginning of the study, the computer crashed and had to be replaced, requiring the entire electronic protocol to be rebuilt. On several occasions, this happened at the time of the assay, rendering those data unreliable as dye-incubation times had to be altered,

sometimes in excess of 20 minutes. At other times, it was difficult to determine if the machine was functioning per specifications, with the proper injection volumes at the proper times, and internal sensors taking the proper readings. The best way to resolve these technical- and user-errors would be to become more familiar with the plate-reader mechanics, set-up, and it's use prior to ever attempting the experiment. Additionally, it may be helpful to develop a quick and inexpensive way to test the function of the plate reader periodically, verifying injection needle and sensor calibration. Overall familiarity and routine maintenance may help to improve work with the plate-reader in the future.

Of course, the current data cannot be dismissed entirely as there are some clear trends among treatment types. Initial addition of UTP appears to have a more potent action on cells exposed to Lipofectamine^{TM} with and without RNA when compared to Co_3O_4NP treatments with and without RNA. This trend is continued during desensitization, with larger initial doses of UTP required to elicit full desensitization upon re-challenge. It is, however, difficult to determine the absolute magnitude of this effect from each treatment as the data from wild type cells does not follow expected trends, most notably at the lowest UTP concentrations where it appears to begin with 50% of a maximal response. As an attempt to account for this, one desensitization trial exposed wild type cells to the standard panel of 10^{-8}-10^{-3} M UTP, in addition to two lower doses of 10^{-9} and 10^{-10} M (data not shown). These additional concentrations reveal the expected sigmoidal dose-response shape curve with a strong left-ward shift: initial incubation with the ligand was more potent in these trials than previously reported by the literature. While it is possible that the expression of this receptor in this cell line has changed some basic physiologic properties over time, these unexpected responses may also be related to malfunction of the machine. For example, if the volume of agonist delivered differed from specifications, or if the

secondary re-challenging dose of UTP were delivered later than the planned 5-minute time frame.

Taken together, the qRT-PCR and calcium assay data indicate that further trials will be required before any reasonable conclusions may be drawn with respect to Co_3O_4NP effectiveness to deliver siRNA into eukaryotic cells. One major shortcoming of this study was the lack of characterization of the nanoparticles. Suspensions were prepared from a stock vial which had been capped but not sealed with parafilm and stored for several years in full light at room temperature. Without characterization of nanoparticle geometry and size by electron microscopy there is no way to tell if they maintained the required characteristics over time. If, for example, over time nanoparticles were able to aggregate forming microscopic structures, they may no longer possess the desired characteristics; the ability to conjugate to nucleic acid and readily enter cells without causing damage. In addition to characterization of the nanoparticles, their conjugation to siRNA should have also been studied. Previously, Hurst & DeLong have shown that Zinc Oxide nanoparticles conjugated to splice-switching oligonucleotides have a specific profile under 2 dimensional fluorescence-difference spectroscopic analysis, unique from that of the naked nanoparticle, which allows for confirmation of this conjugation (66).

REFERENCES

1. Lu, M., and Wu, B. (2016) Structural studies of G protein-coupled receptors. *IUBMB Life*. **68**, 894–903

2. Zhang, H., Unal, H., Gati, C., Han, G. W., Liu, W., Zatsepin, N. A., James, D., Wang, D., Nelson, G., Weierstall, U., Sawaya, M. R., Xu, Q., Messerschmidt, M., Williams, G. J., Boutet, S., Yefanov, O. M., White, T. A., Wang, C., Ishchenko, A., Tirupula, K. C., Desnoyer, R., Coe, J., Conrad, C. E., Fromme, P., Stevens, R. C., Katritch, V., Karnik, S. S., and Cherezov, V. (2015) Structure of the angiotensin receptor revealed by serial femtosecond crystallography. *Cell*. **161**, 833–844

3. Ballesteros, J. A., Jensen, A. D., Liapakis, G., Rasmussen, S. G. F., Shi, L., Gether, U., and Javitch, J. A. (2001) Activation of the β2-Adrenergic Receptor Involves Disruption of an Ionic Lock between the Cytoplasmic Ends of Transmembrane Segments 3 and 6. *J. Biol. Chem.* **276**, 29171–29177

4. Kroeze, W. K., Sassano, M. F., Huang, X.-P., Lansu, K., Mccorvy, J. D., Giguere, P. M., Sciaky, N., and Roth, B. L. PRESTO-TANGO: an open-source resource for interrogation of the druggable human GPCR-ome. doi:10.1038/nsmb.3014

5. Zhang, Y., Devries, M. E., and Skolnick, J. (2006) Structure modeling of all identified G protein-coupled receptors in the human genome. *PLoS Comput. Biol.* **2**, 88–99

6. Pierce, K. L., Premont, R. T., and Lefkowitz, R. J. (2002) Seven-transmembrane receptors. *Nat. Rev. Mol. Cell Biol.* **3**, 639–650

7. Hughes, C. E., and Nibbs, R. J. B. (2018) A guide to chemokines and their receptors. *FEBS J.* **285**, 2944–2971

8. Williams, J. T., Ingram, S. L., Henderson, G., Chavkin, C., von Zastrow, M., Schulz, S., Koch, T., Evans, C. J., and Christie, M. J. (2013) Regulation of μ-opioid receptors: Desensitization, phosphorylation, internalization, and tolerance. *Pharmacol. Rev.* **65**, 223–254

9. Burnstock, G. (2018) Purine and purinergic receptors. *Brain Neurosci. Adv.* **2**, 239821281881749

10. Harmar, A. J. (2001) Family-B G-protein-coupled receptors. *Genome Biol.* **2**, 1–10

11. Niswender, C. M., and Conn, P. J. (2010) Metabotropic glutamate receptors: Physiology, pharmacology, and disease. *Annu. Rev. Pharmacol. Toxicol.* **50**, 295–322

12. Bettler, B., Kaupmann, K., Mosbacher, J., and Gassmann, M. (2004) Molecular structure and physiological functions of GABAB receptors. *Physiol. Rev.* **84**, 835–867

13. MacDonald, B. T., and He, X. (2012) Frizzled and LRP5/6 Receptors for Wnt/ -Catenin Signaling. *Cold Spring Harb. Perspect. Biol.* **4**, a007880–a007880

14. Alexander, S. P. H., Christopoulos, A., Davenport, A. P., Kelly, E., Mathie, A., Peters, J. A., Veale, E. L., Armstrong, J. F., Faccenda, E., Harding, S. D., Pawson, A. J., Sharman, J. L., Southan, C., Davies, J. A., Abbracchio, M. P., Alexander, W., Al-hosaini, K., Bäck, M., Beaulieu, J. M., Bernstein, K. E., Bettler, B., Birdsall, N. J. M., Blaho, V., Bousquet, C., Bräuner-Osborne, H., Burnstock, G., Caló, G., Castaño, J. P., Catt, K. J., Ceruti, S., Chazot, P., Chiang, N., Chun, J., Cianciulli, A., Clapp, L. H., Couture, R., Csaba, Z., Dent, G., Singh, K. D., Douglas, S. D., Dournaud, P., Eguchi, S., Escher, E., Filardo, E., Fong, T. M., Fumagalli, M., Gainetdinov, R. R., Gasparo, M. de, Gershengorn, M., Gobeil, F., Goodfriend, T. L., Goudet, C., Gregory, K. J., Gundlach, A. L., Hamann, J., Hanson, J., Hauger, R. L., Hay, D., Heinemann, A., Hollenberg, M. D., Holliday, N. D., Horiuchi, M., Hoyer, D., Hunyady, L., Husain, A., Ijzerman, A. P., Inagami, T., Jacobson, K. A., Jensen, R. T., Jockers, R., Jonnalagadda, D., Karnik, S., Kaupmann, K., Kemp, J., Kennedy, C., Kihara, Y., Kozielewicz, P., Kreienkamp, H. J., Kukkonen, J. P., Langenhan, T., Leach, K., Lecca, D., Lee, J. D., Leeman, S. E., Leprince, J., Lolait, S. J., Lupp, A., Macrae, R., Maguire, J., Mazella, J., McArdle, C. A., Melmed, S., Michel, M. C., Miller, L., Mitolo, V., Mouillac, B., Murphy, P. M., Nahon, J. L., Norel, X., Nyimanu, D., O'Carroll, A. M., Offermanns, S., Panaro, M. A., Pertwee, R. G., Pin, J. P., Prossnitz, E., Ramachandran, R., Reinscheid, R. K., Rondard, P., Rovati, G. E., Ruzza, C., Sanger, G., Schöneberg, T., Schulte, G., Schulz, S., Segaloff, D. L., Serhan, C. N., Stoddart, L. A., Sugimoto, Y., Summers, R., Tan, V., Thomas, W., Timmermans, P. B. M. W. M., Tirupula, K., Tulipano, G., Unal, H., Unger, T., Vanderheyden, P., Vaudry, D., Vaudry, H., Vilardaga, J. P., Walker, C. S., Ward, D. T., Wester, H. J., Willars, G. B., Williams, T. L., Woodruff, T. M., and Yao, C. (2019) THE CONCISE GUIDE TO PHARMACOLOGY 2019/20: G protein-coupled receptors. *Br. J. Pharmacol.* **176**, S21–S141

15. Harding, S. D., Armstrong, J. F., Faccenda, E., Southan, C., Alexander, S. P. H., Davenport, A. P., Pawson, A. J., Spedding, M., and Davies, J. A. (2022) The IUPHAR/BPS guide to PHARMACOLOGY in 2022: curating pharmacology for COVID-19, malaria and antibacterials. *Nucleic Acids Res.* **50**, D1282–D1294

16. Kamato, D., Thach, L., Bernard, R., Chan, V., Zheng, W., Kaur, H., Brimble, M., Osman, N., and Little, P. J. (2015) Structure, Function, Pharmacology, and Therapeutic Potential of the G Protein, Gα/q,11. *Front. Cardiovasc. Med.* **2**, 1–11

17. Buhl, A. M., Johnson, N. L., Dhanasekaran, N., and Johnson, G. L. (1995) Gα12 and Gα13 stimulate Rho-dependent stress fiber formation and focal adhesion assembly. *J. Biol. Chem.* **270**, 24631–24634

18. Marrari, Y., Crouthamel, M., Irannejad, R., and Wedegaertner, P. B. (2007) Assembly and trafficking of heterotrimeric G proteins. *Biochemistry*. **46**, 7665–7677

19. Krapivinsky, G., Krapivinsky, L., Wickman, K., and Clapham, D. E. (1995) Gβγ binds directly to the G protein-gated K+ channel, I(KACh). *J. Biol. Chem.* **270**, 29059–29062

20. Boyer, J. L., Waldo, G. L., and Harden, T. K. (1992) βγ-Subunit activation of G-protein-regulated phospholipase C. *J. Biol. Chem.* **267**, 25451–25456

21. Ito, A., Satoh, T., Kaziro, Y., and Itoh, H. (1995) G protein βγ subunit activates Ras, Raf, and MAP kinase in HEK 293 cells. *FEBS Lett.* **368**, 183–187

22. Campbell, A. P., and Smrcka, A. V. (2018) Targeting G protein-coupled receptor signalling by blocking G proteins. *Nat. Rev. Drug Discov.* **17**, 789–803

23. Van Unen, J., Woolard, J., Rinken, A., Hoffmann, C., Hill, S. J., Goedhart, J., Bruchas, M. R., Bouvier, M., and Adjobo-Hermans, M. J. W. (2015) A perspective on studying G-protein-coupled receptor signaling with resonance energy transfer biosensors in living organisms. *Mol. Pharmacol.* **88**, 589–595

24. Ayoub, M. A., Al-Senaidy, A., and Pin, J. P. (2012) Receptor-G protein interaction studied by bioluminescence resonance energy transfer: Lessons from protease-activated receptor 1. *Front. Endocrinol. (Lausanne).* **3**, 1–13

25. Dean, M., Hamon, Y., and Chimini, G. (2001) The human ATP-binding cassette (ABC) transporter superfamily. *J. Lipid Res.* **42**, 1007–1017

26. Baker, D. A., and Kelly, J. M. (2004) Structure, function and evolution of microbial adenylyl and guanylyl cyclases. *Mol. Microbiol.* **52**, 1229–1242

27. Nirody, J. A., Budin, I., and Rangamani, P. (2020) ATP synthase: Evolution, energetics, and membrane interactions. *J. Gen. Physiol.* 10.1085/JGP.201912475

28. Burnstock, G., Campbell, G., Satchell, D., and Smythe, A. (1970) *Evidence that adenosine triphosphate or a related nucleotide is the transmitter substance released by non-adrenergic inhibitory nerves in the gut. Br. J. Pharmac.* **40,** 668-688

29. Burnstock, G., and Verkhratsky, A. (2012) Early History of Purinergic Signalling. in *Purinergic Signalling and the Nervous System*, pp. 7–66, Springer Berlin Heidelberg, 10.1007/978-3-642-28863-0_2

30. Elliott, M. R., Chekeni, F. B., Trampont, P. C., Lazarowski, E. R., Kadl, A., Walk, S. F., Park, D., Woodson, R. I., Ostankovich, M., Sharma, P., Lysiak, J. J., Harden, T. K., Leitinger, N., and Ravichandran, K. S. (2009) Nucleotides released by apoptotic cells act as a find-me signal to promote phagocytic clearance. *Nature*. **461**, 282–286

31. Burnstock, G. (2007) Physiology and pathophysiology of purinergic neurotransmission. *Physiol. Rev.* **87**, 659–797

32. Burnstock, G. (2011) Introductory overview of purinergic signalling. *Front Biosci* **E3**, 896-900

33. Burnstock, G. (2014) Purinergic Signalling in the CNS. *Open Neurosci. J.* **4**, 24–30

34. Jacobson, K. A., and Gao, Z. G. (2006) Adenosine receptors as therapeutic targets. *Nat. Rev. Drug Discov.* **5**, 247–264

35. North, R. A. (2016) P2X receptors. *Philos. Trans. R. Soc. Lond. B. Biol. Sci.* 10.1098/rstb.2015.0427

36. Erb, L., Liao, Z., Seye, C. I., and Weisman, G. A. (2006) P2 receptors: Intracellular signaling. *Pflugers Arch. Eur. J. Physiol.* **452**, 552–562

37. Kolen, K., and Slegers, H. (2006) Integration of P2Y receptor-activated signal transduction pathways in G protein-dependent signalling networks. *Purinergic Signal.* **2**, 451–469

38. Erb, L., and Weisman, G. A. (2012) Coupling of P2Y receptors to G proteins and other signaling pathways. *Wiley Interdiscip. Rev. Membr. Transp. Signal.* 10.1002/wmts.62

39. Kennedy, C. That was then, this is now: the development of our knowledge and understanding of P2 receptor subtypes. 10.1007/s11302-021-09763-0/Published

40. Davalos, D., Grutzendler, J., Yang, G., Kim, J. V., Zuo, Y., Jung, S., Littman, D. R., Dustin, M. L., and Gan, W. B. (2005) ATP mediates rapid microglial response to local brain injury in vivo. *Nat. Neurosci.* **8**, 752–758

41. Abbracchio, M. P., and Ceruti, S. (2006) Roles of P2 receptors in glial cells: Focus on astrocytes. *Purinergic Signal.* **2**, 595–604

42. Brambilla, R., and Abbracchio, M. P. (2001) Modulation of cyclooxygenase-2 and brain reactive astrogliosis by purinergic P2 receptors. *Ann. N. Y. Acad. Sci.* **939**, 54–62

43. Garrad, R. C., Otero, M. A., Erb, L., Theiss, P. M., Clarke, L. L., Gonzalez, F. A., Turner, J. T., and Weisman, G. A. (1998) Structural Basis of Agonist-induced Desensitization and Sequestration of the P2Y 2 Nucleotide Receptor. *J. Biol. Chem.* **273**, 29437–29444

44. Flores, R. V., Hernández-Pérez, M. G., Aquino, E., Garrad, R. C., Weisman, G. A., and Gonzalez, F. A. (2005) Agonist-induced phosphorylation and desensitization of the P2Y2 nucleotide receptor. *Mol. Cell. Biochem.* **280**, 35–45

45. Lefkowitz, R. J., Rajagopal, K., and Whalen, E. J. (2006) New Roles for ??-Arrestins in Cell Signaling: Not Just for Seven-Transmembrane Receptors. *Mol. Cell*. 10.1016/j.molcel.2006.11.007

46. Ma, L., and Pei, G. (2007). Beta-arrestin signaling and regulation of transcription. *J. Cell Sci. 120*(Pt 2), 213–218. https://doi.org/10.1242/jcs.03338

47. Schmid, S. L. (2002) Clathrin-coated vesicle formation and protein sorting: An Integrated Process. *Annu. Rev. Biochem.* **66**, 511–548

48. Stoffel, R. H., Randall, R. R., Premont, R. T., Lefkowitz, R. J., and Inglese, J. (1994) Palmitoylation of G protein-coupled receptor kinase, GRK6. *J. Biol. Chem.* **269**, 27791–27794

49. Premont, R. T., Macrae, A. D., Stoffel, R. H., Chung, N., Pitcher, J. A., Ambrose, C., Inglese, J., MacDonald, M. E., and Lefkowitz, R. J. (2002) Characterization of the G Protein-coupled Receptor Kinase GRK4. *J. Biol. Chem.* **271**, 6403–6410

50. Stoffel, R. H., Inglese, J., Macrae, A. D., Lefkowitz, R. J., and Premont, R. T. (1998) Palmitoylation increases the kinase activity of the G protein-coupled receptor kinase, GRK6. *Biochemistry*. **37**, 16053–16059

51. Boekhoff, I., Inglese, J., Schleicher, S., Koch, W. J., Lefkowitz, R. J., and Breer, H. (1994) Olfactory desensitization requires membrane targeting of receptor kinase mediated by βγ-subunits of heterotrimeric G proteins. *J. Biol. Chem.* **269**, 37–40

52. Sato, P. Y., Chuprun, J. K., Schwartz, M., and Koch, W. J. (2015) The Evolving Impact of G Protein-Coupled Receptor Kinases in Cardiac Health and Disease. *Physiol. Rev.* **95**, 377–404

53. Motegi, S. I. (2016) Endothelin. *Syst. Scler.* 10.1007/978-4-431-55708-1_10

54. Alvarez, C. E. (2008) On the origins of arrestin and rhodopsin. *BMC Evol. Biol.* **8**, 1–13

55. Oakley, R. H., Laporte, S. A., Holt, J. A., Caron, M. G., and Barak, L. S. (2000) Differential affinities of visual arrestin, βarrestin1, and βarrestin2 for G protein-coupled receptors delineate two major classes of receptors. *J. Biol. Chem.* **275**, 17201–17210

56. Thomsen, A. R. B., Plouffe, B., Cahill, T. J., Shukla, A. K., Tarrasch, J. T., Dosey, A. M., Kahsai, A. W., Strachan, R. T., Pani, B., Mahoney, J. P., Huang, L., Breton, B., Heydenreich, F. M., Sunahara, R. K., Skiniotis, G., Bouvier, M., Lefkowitz, R. J., and Lefkowitz, R. J. (2016) GPCR-G Protein-β-Arrestin Super-Complex Mediates Sustained G Protein Signaling. *Cell*. **166**, 907–919

57. Cahill, T. J., Thomsen, A. R. B., Tarrasch, J. T., Plouffe, B., Nguyen, A. H., Yang, F., Huang, L.-Y., Kahsai, A. W., Bassoni, D. L., Gavino, B. J., Lamerdin, J. E., Triest, S., Shukla, A. K., Berger, B., Little, J., Antar, A., Blanc, A., Qu, C.-X., Chen, X., Kawakami, K., Inoue, A., Aoki, J., Steyaert, J., Sun, J.-P., Bouvier, M., Skiniotis, G., and Lefkowitz, R. J. (2017) Distinct conformations of GPCR–β-arrestin complexes mediate desensitization, signaling, and endocytosis. *Proc. Natl. Acad. Sci.* **114**, 2562–2567

58. Violin, J. D., and Lefkowitz, R. J. (2007) β-Arrestin-biased ligands at seven-transmembrane receptors. *Trends Pharmacol. Sci.* **28**, 416–422

59. Reiter, E., Ahn, S., Shukla, A. K., and Lefkowitz, R. J. (2012) Molecular mechanism of β-arrestin-biased agonism at seven-transmembrane receptors. *Annu. Rev. Pharmacol. Toxicol.* **52**, 179–197

60. Bohn, L. M., Lefkowitz, R. J., and Caron, M. G. (2002) Differential mechanisms of morphine antinociceptive tolerance revealed in βarrestin-2 knock-out mice. *J. Neurosci.* **22**, 10494–10500

61. Raehal, K. M., Walker, J. K. L., and Bohn, L. M. (2005) Morphine side effects in β-arrestin 2 knockout mice. *J. Pharmacol. Exp. Ther.* **314**, 1195–1201

62. Sokolova, V., and Epple, M. (2008) Inorganic nanoparticles as carriers of nucleic acids into cells. *Angew. Chemie - Int. Ed.* **47**, 1382–1395

63. Cappellini, F., Hedberg, Y., McCarrick, S., Hedberg, J., Derr, R., Hendriks, G., Odnevall Wallinder, I., and Karlsson, H. L. (2018) Mechanistic insight into reactivity and (geno)toxicity of well-characterized nanoparticles of cobalt metal and oxides. *Nanotoxicology*. **12**, 602–620

64. Dean, J. M. (2014) *Splice Switching Oligonucleotides: Model System Splice Switching Oligonucleotides: Model System Characterization, Nanomaterial Delivery, and Rational Design for Characterization, Nanomaterial Delivery, and Rational Design for Targeting Melanoma at the RNA.* Master's thesis, Missouri State University

65. Papis, E., Rossi, F., Raspanti, M., Dalle-Donne, I., Colombo, G., Milzani, A., Bernardini, G., and Gornati, R. (2009) Engineered cobalt oxide nanoparticles readily enter cells. *Toxicol. Lett.* 10.1016/j.toxlet.2009.06.851

66. Hurst, M. N., and DeLong, R. K. (2016) Two-Dimensional Fluorescence Difference Spectroscopy to Characterize Nanoparticles and their Interactions. *Sci. Rep.* 10.1038/srep33287

67. Weaver, R. F. (2012) *Molecular Biology*, 6th ed., New York: McGraw-Hill

68. Louiselle, D. A. (2014) *Development of a microplate-based calcium assay for studying desensitization of the P2Y2 nucleotide receptor.* Master's thesis, Missouri State University

69. Luttrell, L. M., and Lefkowitz, R. J. (2002) The role of β-arrestins in the termination and transduction of G-protein-coupled receptor signals. *J. Cell Sci.* **115**, 455–465

70. Chattopadhyay, S., Chakraborty, S. P., Laha, D., Baral, R., Pramanik, P., and Roy, S. (2012) Surface-modified cobalt oxide nanoparticles: New opportunities for anti-cancer drug development. *Cancer Nanotechnol.* **3**, 13–23

71. Xiaowei Wang, B. S. (2003) A PCR primer bank for quantitative gene expression analysis. *Nucleic Acids Res.*

72. Athanasia Spandidos, Xiaowei Wang, Huajun Wang, B. S. (2010) No Title. *Prim. a Resour. Hum. mouse PCR Prim. pairs gene Expr. Detect. Quantif.*

73. Athanasia Spandidos, Xiaowei Wang, Huajun Wanf, Stefan Dragnev, Tara Thurber, B. S. (2008) No Title. *A Compr. Collect. Exp. calidated Prim. Polmerase Chain React.*

74. Suleymanova, N., Crudden, C., Shibano, T., Worrall, C., Oprea, I., Tica, A., Calin, G. A., Girnita, A., and Girnita, L. (2017) Functional antagonism of β-arrestin isoforms balance IGF-1R expression and signalling with distinct cancer-related biological outcomes. *Oncogene*. **36**, 5734–574

APPENDICES

Appendix A: qRT-PCR Calculations, cDNA 1

	GAPDH		β-arrestin1		Calculations	
	C_t	SQ	C_t	SQ	ΔSQ	ΔΔSQ
Wild Type	26.77	15.41	34.12	0.08655	0.00564	1.10815
	26.92	13.88	36.04	0.02226	0.00145	0.28501
	26.66	16.71	33.59	0.12550	0.00818	1.60685
Lipofectamine^{TM} Vehicle	27.91	6.89	35.76	0.02726	0.00362	0.70987
	27.45	9.54	35.18	0.04086	0.00542	1.06402
	28.07	6.19	33.9	0.10090	0.01338	2.62751
Cobalt Vehicle	24.92	57.18	34.78	0.05422	0.00064	0.12551
	23.68	136.40	34.47	0.06760	0.00080	0.15648
	24.83	60.86	33.45	0.13870	0.00164	0.32105
Lipofectamine^{TM} + siRNA	23.49	156.20	34.45	0.06832	0.00021	0.04135
	23.33	175.10	34.23	0.07984	0.00025	0.04832
	21.49	641.80	34.13	0.08555	0.00026	0.05178
Co_3O_4NP 180 µg/ml + siRNA	23.49	156.70	34.29	0.07655	0.00039	0.07567
	22.23	379.10	34.47	0.06754	0.00034	0.06677
	24.85	59.98	34.08	0.08870	0.00045	0.08769
Co_3O_4NP 90 µg/ml + siRNA	24.7	66.75	35.27	0.03830	0.00087	0.17064
	25.87	29.16	34.65	0.05951	0.00135	0.26514
	25.56	36.28	35.01	0.04614	0.00105	0.20557
Co_3O_4NP 45 µg/ml + siRNA	21.31	729.00	32.6	0.25240	0.00074	0.14432
	23.56	148.80	35.04	0.04511	0.00013	0.02579
	23.53	152.20	32.81	0.21840	0.00064	0.12488
Co_3O_4NP 25 µg/ml + siRNA	24.03	106.60	32.75	0.22760	0.00181	0.35547
	23.95	112.90	31.97	0.39450	0.00314	0.61614
	23.48	157.60	32.61	0.25040	0.00199	0.39108

Appendix B: qRT-PCR Calculations, cDNA 2

	GAPDH		β-arrestin1		Calculations	
	C_t	SQ	C_t	SQ	ΔSQ	ΔΔSQ
Wild Type	26.87	15.69	34.96	0.09345	0.00632	0.67126
	27.02	14.28	34.07	0.16460	0.01113	1.18233
	27.01	14.39	34.12	0.15960	0.01079	1.14641
Lipofectamine™ Vehicle	26.55	19.20	34.24	0.14760	0.00744	0.79071
	26.45	20.43	34.01	0.17080	0.00861	0.91499
	26.5	19.85	33.3	0.26730	0.01348	1.43195
Cobalt Vehicle	26.67	17.83	33.94	0.17850	0.01043	1.10829
	26.77	16.73	32.87	0.35210	0.02058	2.18615
	26.77	16.76	33.11	0.30110	0.01760	1.86950
Lipofectamine™ + siRNA	22.17	308.30	33.28	0.27030	0.00090	0.09548
	22.22	298.50	31.98	0.61730	0.00205	0.21804
	22.23	295.30	33.26	0.27390	0.00091	0.09675
Co_3O_4NP 180 µg/ml + siRNA	29.84	2.39	34.72	0.10910	0.04465	4.74265
	29.83	2.40	35.12	0.08445	0.03456	3.67110
	29.75	2.53	35.48	0.06714	0.02748	2.91862
Co_3O_4NP 90 µg/ml + siRNA	29.28	3.41	35.1	0.08549	0.02557	2.71563
	29.24	3.50	34.34	0.13820	0.04133	4.39000
	29.42	3.12	33.63	0.21680	0.06484	6.88677
Co_3O_4NP 45 µg/ml + siRNA	26.88	15.55	34.94	0.09469	0.00584	0.62070
	26.84	16.01	34.24	0.14750	0.00910	0.96687
	26.74	17.05	33.79	0.19680	0.01215	1.29003
Co_3O_4NP 25 µg/ml + siRNA	26.3	22.50	34.29	0.14280	0.0632	0.67141
	26.4	21.19	34.65	0.11380	0.00504	0.53506
	26.19	24.08				

Appendix C: qRT-PCR Calculations, cDNA 3

	GAPDH		β-arrestin1		Calculations	
	C_t	SQ	C_t	SQ	ΔSQ	ΔΔSQ
Wild Type	24.31	67.55	35.49	0.06833	0.00077	0.75751
	23.3	125.60	34.73	0.10900	0.00123	1.20838
	24.19	72.41	34.99	0.09328	0.00105	1.03411
Lipofectamine™ Vehicle	22.84	167.40	35.39	0.07254	0.00053	0.52474
	27.63	8.68	35.37	0.07359	0.00054	0.53234
	22.31	230.90	33.75	0.20010	0.00148	1.44749
Cobalt Vehicle	25.62	29.97	34.84	0.10170	0.00718	7.04370
	27.7	8.35	34.56	0.12090	0.00853	8.37348
	28.82	4.19	33.78	0.19610	0.01384	13.58180
Lipofectamine + siRNA	26.48	17.73	34.2	0.15100	0.00785	7.70578
	27.18	11.50	35.05	0.08940	0.00465	4.56223
	25.71	28.46	36.09	0.04726	0.00246	2.41176
Co_3O_4NP 180 µg/ml + siRNA	23.71	97.46	33.41	0.24710	0.00102	0.99938
	20.8	589.20	34.77	0.10630	0.00044	0.42992
	25.11	41.26	34	0.17170	0.00071	0.69443
Co_3O_4NP 90 µg/ml + siRNA	22.16	254.40	35.21	0.08110	0.00019	0.18900
	20.2	849.20	34.19	0.15250	0.00036	0.35539
	22.91	159.70	35.29	0.07726	0.00018	0.18005
Co_3O_4NP 45 µg/ml + siRNA	25.76	27.66	35.25	0.07904	0.00368	3.60980
	25.86	25.93	34.74	0.10860	0.00368	3.60980
	25.37	34.98	34.26	0.14630	0.00496	4.86293
Co_3O_4NP 25 µg/ml + siRNA	23.47	113.10	34.54	0.12250	0.00207	2.03454
	25.82	26.50	35.14	0.08495	0.00144	1.41089
	25.25	37.66	34.86	0.10080	0.00171	1.67413

Appendix D: qRT-PCR Calculations, cDNA 4

	GAPDH		β-arrestin1		Calculations	
	C_t	SQ	C_t	SQ	ΔSQ	ΔΔSQ
Wild Type	18.92	446200	30.51	53.090	0.000172	1.39852
	19.71	241600	31.4	26.630	0.000086	0.49050
	19.72	239300	31.21	30.900	0.000100	1.11098
Lipofectamine™ Vehicle	18.97	428900	30.44	56.040	0.000138	2.89221
	19.23	351600	31.43	25.920	0.000064	1.33772
	18.94	439600	31.03	35.460	0.000087	1.83008
Cobalt Vehicle	21.31	69620	31.93	17.6300	0.000278	2.33385
	21.89	44120	33.84	3.9650	0.000063	0.52488
	21.19	76190	32.62	10.3100	0.000163	1.36483
Lipofectamine + siRNA	18.75	511200	32.26	13.6100	0.000031	0.25997
	19.05	404300	32.56	10.7300	0.000024	0.20496
	19.06	400800	32.46	11.6500	0.000027	0.22253
Co_3O_4NP 180 µg/ml + siRNA	19.31	329500	32.78	9.097	0.000030	0.62502
	19.71	241100	34.44	2.496	0.000008	0.17149
	19.25	345900	34.14	3.154	0.000010	0.21670
Co_3O_4NP 90 µg/ml + siRNA	21.19	76070	33.32	5.941	0.000067	1.40243
	21.25	72880	34.51	2.362	0.000027	0.55757
	20.63	117800	34.98	1.627	0.000018	0.38407
Co_3O_4NP 45 µg/ml + siRNA	18.15	812400	31.34	27.930	0.000038	0.78888
	18.54	600900	32.22	14.090	0.000019	0.39797
	18.15	816100	32.4	12.230	0.000016	0.34543
Co_3O_4NP 25 µg/ml + siRNA	19.08	394300	31.35	27.670	0.000075	1.57879
	19.35	320300	33.04	7.386	0.000020	0.42143
	19.1	389000	32.45	11.730	0.000032	0.66929

Appendix E: Threshold Cycle for GAPDH and β-arrestin1

Threshold Cycle (Ct) of 3 replicates, anchored at the mean and showing SEM. Shaded points indicate GAPDH target, open points for β-arrestin1 target.

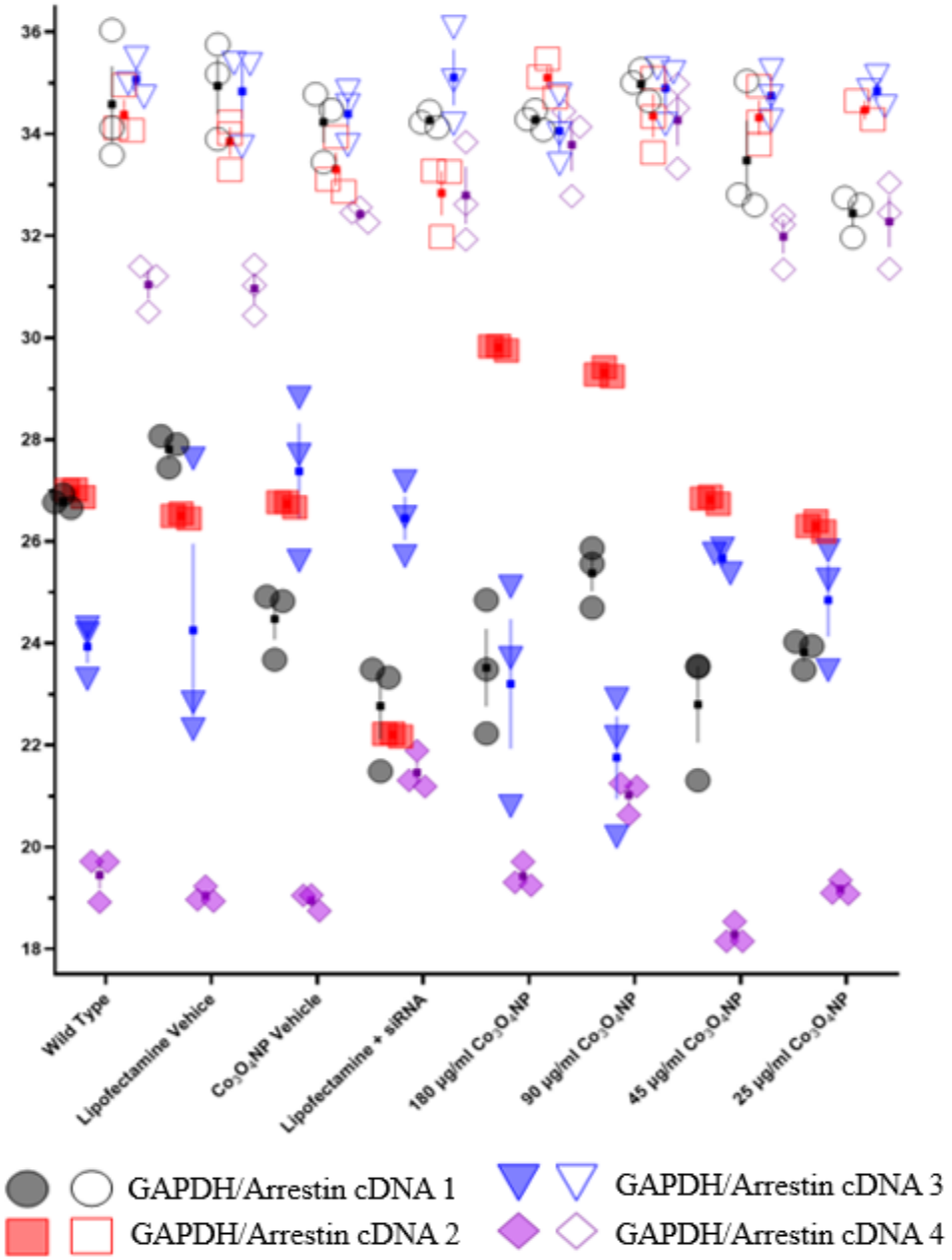

Appendix F: Percent of Maximal Change in Fluorescence, Activation

	Wild Type	Lipofectamine™		Co_3O_4NP	
siRNA	(-)	(-)	(+)	(-)	(+)
-8	25 31 41 46 47 55 44 16	0.0 6.8 11 5.3 1.5 5.3	3.0 0.9 1.9 2.8 1.3 1.9	7.7 0.9 3.4 0.0 2.0 9.1	8.8 4.1 5.2 0.0 15 0.3
-7	62 35 48 24 42 78 45 38	1.0 13 9.8 8.6 7.8 12	10 6.4 7.7 7.2 9.6 0.9	5.7 3.4 3.4 2.8 1.1 3.7	4.4 5.5 3.9 6.1 2.5 3.9
-6	49 61 57 51 61 53 41 33	30 36 51 58 78 36	56 51 44 43 42 30	19 14 16 11 11 16	13 29 15 21 17 26
-5	48 53 68 67 64 64 53 45	39 70 59 77 80 93	86 40 56 51 59 41	59 57 60 65 40 28	28 42 55 100 53 63
-4	77 75 73 54 69 87 54 41	53 78 96 75 74 100	77 76 60 55 69 44	68 83 63 70 88 43	51 46 63 69 82 75
-3	62 71 69 100 68 64 55 69	58 100 84 81 84 54	64 54 41 100 53 30	90 88 74 100 78 75	66 64 84 83 92 94

Appendix G: Percent of Maximal Change in Fluorescence, Desensitization.

	Wild Type	Lipofectamine™		Co_3O_4NP	
siRNA	(-)	(-)	(+)	(-)	(+)
-8	100 75 79 94 66 12 49 28	33 77 71 69 68 78	72 71 53 74 68 62	81 75 74 55 38 40	44 62 87 62 76 39
-7	17 24 12 35 13 13 10 7	37 98 84 100 85 92	90 100 90 89 65 76	75 68 36 100 58 27	40 67 80 87 72 75
-6	2.9 3.8 9.7 3.6 5.5 5.5 2.1 0.0	21 59 42 46 32 41	20 25 30 27 24 30	85 62 45 77 8.1 31	35 60 64 100 71 86
-5	3.4 6.7 5.5 7.6 4.5 6.0 5.0 2.4	1.0 3.3 18 5.7 0.0 11	5.7 13 13 1.4 2.4 5.2	13 35 2.3 10 36 19	8.1 29 28 8.5 21 5.3
-4	1.0 4.1 12 7.1 3.8 5.9 7.2 5.7	4.8 3.3 3.8 1.0 1.9 0.0	1.4 1.4 1.0 2.9 0.0 0.5	5.0 4.2 3.8 2.7 4.2 0.0	0.0 8.1 6.4 4.6 4.2 4.9
-3	6.4 7.6 4.8 3.6 6.7 4.8 8.1 0.5	10 2.4 9.1 9.6 3.8 6.2	4.8 6.2 5.7 5.2 4.3 5.7	4.2 0.8 3.8 3.5 6.5 1.5	1.1 6.7 6.7 1.4 7.1 6.4